AD-A072 200 DAVID W TAYLOR NAVAL SHIP RESEARCH AND DEVELOPMENT CE--ETC F/G 20/4
AN INTEGRAL PREDICTION METHOD FOR THREE-DIMENSIONAL TURBULENT B--ETC(U)
JUL 79 C VON KERCZEK, T J LANGAN

UNCLASSIFIED DTNSRDC-79/006 NL

| OF |
AD
A072 00

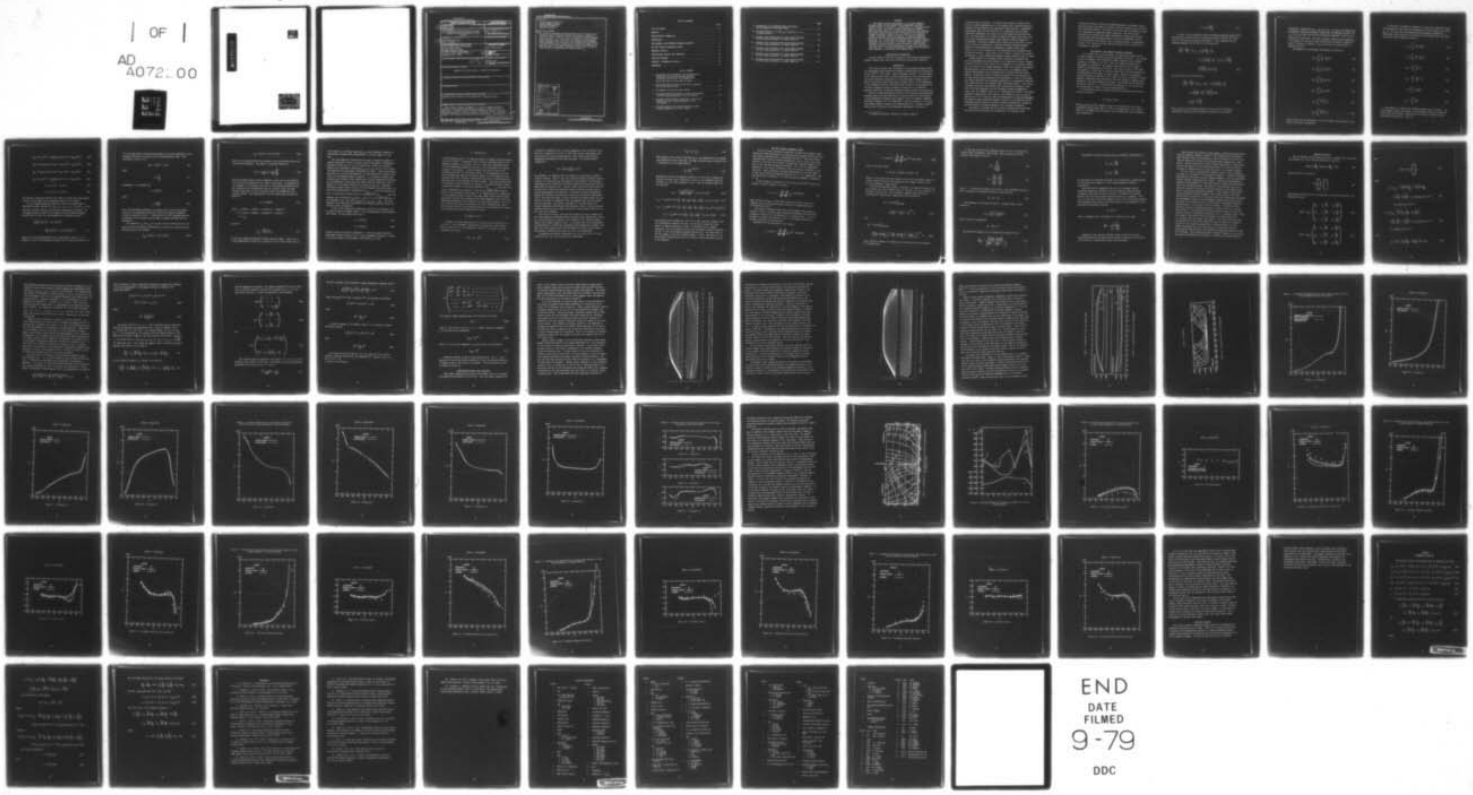

END
DATE
FILMED
9-79
DDC

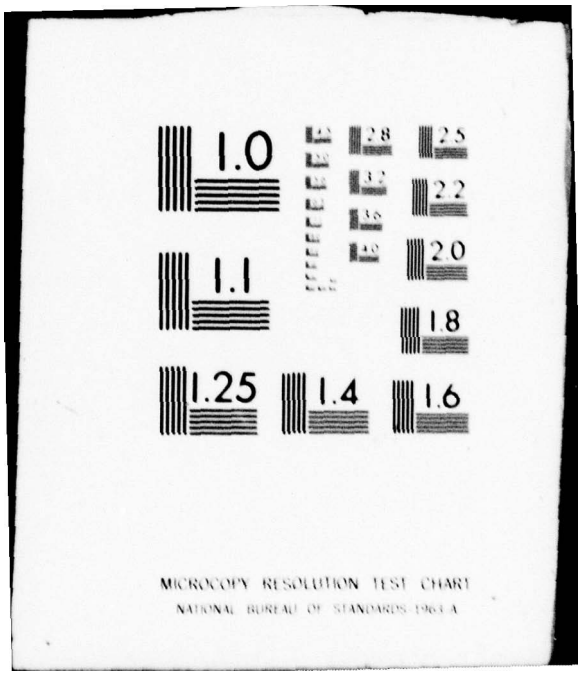
1.0
1.1
1.25
1.4
1.6
2.8
3.2
3.6
4.0
2.5
2.2
2.0
1.8
MICROCOPY RESOLUTION TEST CHART
NATIONAL BUREAU OF STANDARDS 1963 A

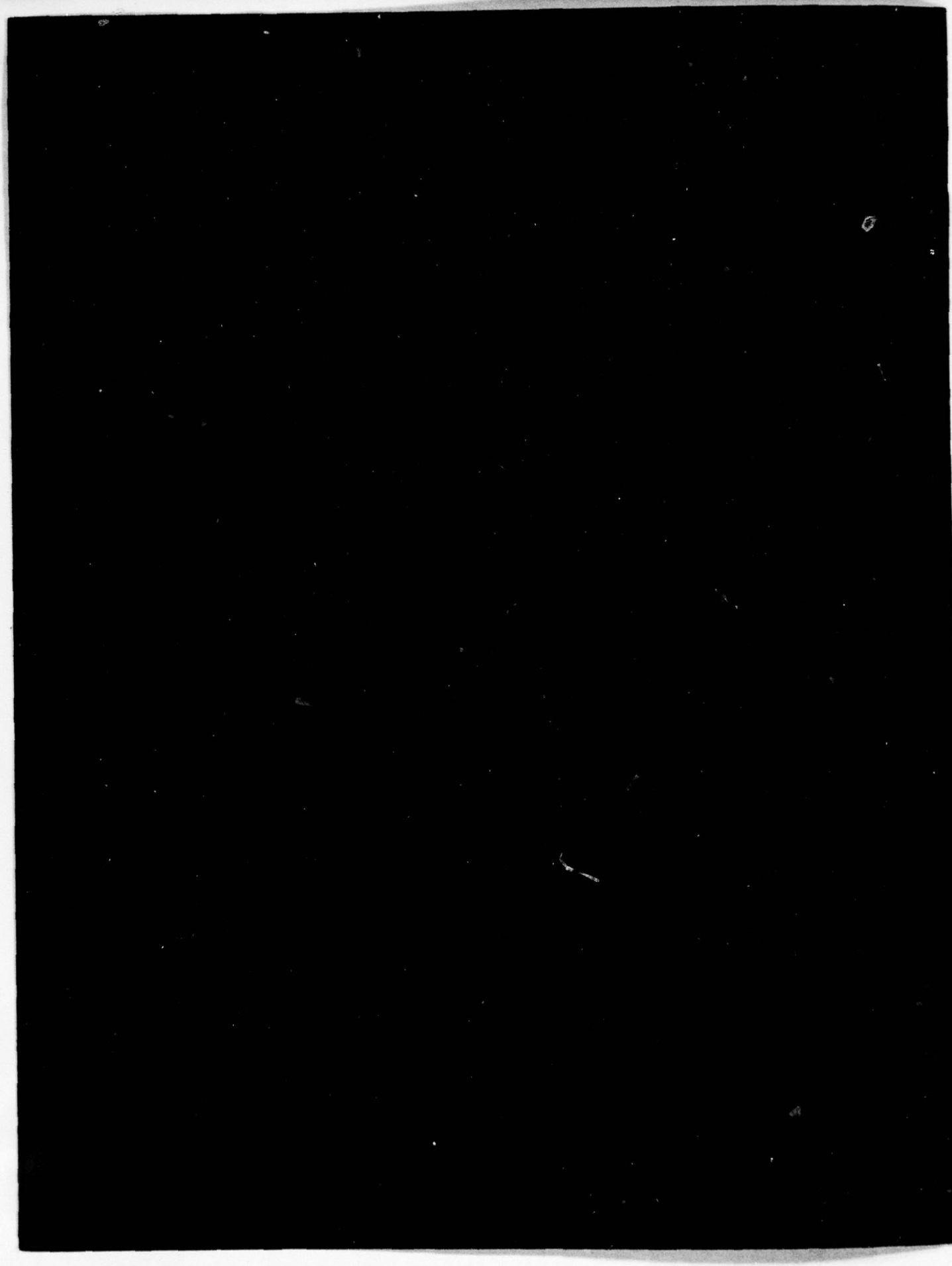

UNCLASSIFIED

SECURITY CLASSIFICATION OF THIS PAGE (When Data Entered)

REPORT DOCUMENTATION PAGE

READ INSTRUCTIONS BEFORE COMPLETING FORM

1. REPORT NUMBER: DTNSRDC-79/006
2. GOVT ACCESSION NO.:
3. RECIPIENT'S CATALOG NUMBER:

4. TITLE (and Subtitle): AN INTEGRAL PREDICTION METHOD FOR THREE-DIMENSIONAL TURBULENT BOUNDARY LAYERS ON SHIPS
5. TYPE OF REPORT & PERIOD COVERED: Final rept.,
6. PERFORMING ORG. REPORT NUMBER:

7. AUTHOR(s): Christian von Kerczek, Thomas J. Langan
8. CONTRACT OR GRANT NUMBER(s):

9. PERFORMING ORGANIZATION NAME AND ADDRESS: David W. Taylor Naval Ship Research and Development Center, Bethesda, Maryland 20084
10. PROGRAM ELEMENT, PROJECT, TASK AREA & WORK UNIT NUMBERS: (See reverse side)

11. CONTROLLING OFFICE NAME AND ADDRESS: Naval Sea Systems Command (SEA-035), Washington, D.C. 20362
12. REPORT DATE: Jul[illegible]79
13. NUMBER OF PAGES: 78

14. MONITORING AGENCY NAME & ADDRESS(if different from Controlling Office): 77 p.
15. SECURITY CLASS. (of this report): UNCLASSIFIED
15a. DECLASSIFICATION/DOWNGRADING SCHEDULE:

16. DISTRIBUTION STATEMENT (of this Report)

APPROVED FOR PUBLIC RELEASE: DISTRIBUTION UNLIMITED

17. DISTRIBUTION STATEMENT (of the abstract entered in Block 20, if different from Report)

18. SUPPLEMENTARY NOTES

19. KEY WORDS (Continue on reverse side if necessary and identify by block number)

Boundary layers, turbulent, three-dimensional, momentum integral

20. ABSTRACT (Continue on reverse side if necessary and identify by block number)

This report presents refinements of a previous momentum-integral method for calculating three-dimensional turbulent boundary layers on ship hulls. In particular the following refinements are made: the small crossflow assumption is removed; numerical calculation of the double model potential flow replaces the slender body potential flow; a more general

(Continued on reverse side)

DD FORM 1 JAN 73 1473 EDITION OF 1 NOV 65 IS OBSOLETE S/N 0102-LF-014-6601

387 682

UNCLASSIFIED

SECURITY CLASSIFICATION OF THIS PAGE (When Data Entered)

(Block 10)

Program Element 61153 N 23
Project Number SR 02301
Task Area SR 023-01-01
Work Unit 1552-070

(Block 20 continued)

and versatile orthogonal coordinate system is used in place of the streamline surface coordinate system; and finally, an improved numerical method is used for solving the momentum-integral boundary-layer equations. It is shown that the boundary layer calculation method, developed here, can be used to calculate certain boundary layer parameters, such as boundary layer thickness or skin friction, with fair accuracy over a large portion of hulls that maintain unseparated flow. The surface coordinate system can also be used in other methods for calculating the boundary layer.

TABLE OF CONTENTS

LIST OF FIGURES

ABSTRACT

This report presents refinements of a previous momentum-integral method for calculating three-dimensional turbulent boundary layers on ship hulls. In particular the following refinements are made: the small crossflow assumption is removed; numerical calculation of the double model potential flow replaces the slender body potential flow; a more general and versatile orthogonal coordinate system is used in place of the streamline surface coordinate system; and finally, an improved numerical method is used for solving the momentum-integral boundary-layer equations. It is shown that the boundary layer calculation method, developed here, can be used to calculate certain boundary layer parameters, such as boundary layer thickness or skin friction, with fair accuracy over a large portion of hulls that maintain unseparated flow. The surface coordinate system can also be used in other methods for calculating the boundary layer.

ADMINISTRATIVE INFORMATION

The work reported herein was supported by the General Hydromechanics Research Program under Task Area SR 023-01-01 and Work Unit 1552-070.

INTRODUCTION

This report presents some refinements of the momentum-integral method for calculating three-dimensional turbulent boundary-layers as developed by von Kerczek[1*] for ship hulls. These refinements include: (1) the removal of the boundary-layer small crossflow approximation; (2) the incorporation of an exact numerical calculation of the double model potential flow instead of using the slender-body theory potential flow; (3) the abandonment of the streamline surface coordinate system in favor of a more general and versatile orthogonal surface coordinate system; and (4) an improved numerical method for solving the momentum-integral boundary layer equations.

The use of momentum-integral methods for calculating three-dimensional boundary layers has come under severe criticism recently by the advocates of the differential boundary layer equations (see, for example, Landweber and Patel,[2] Cebeci et al.[3] and Spalding[4]). The main objection to the integral methods seems to center on the unavailability of a suitable crossflow velocity profile function that adaquately approximates a variety of

*A complete listing of references is given on page 67.

crossflow velocity profiles. It is most often claimed by these critics that an accurate representation of the boundary layer crossflow profile is required for the prediction of longitudinal bilge vortices. Large-scale longitudinal bilge vortices arise due to a complicated form of three-dimensional separation; the vortex flow itself being the separated flow. Thus, one cannot expect to be able to compute the bilge vortex flow, even by the most sophisticated boundary layer methods, whether integral or differential. Presently, boundary layer theory can be used only to calculate the flow up to separation. Recently developed momentum-integral methods for two-dimensional and axisymmetric boundary layers (see Green et al.[5]) are as accurate as, yet considerably more economical than, differential methods. There seems to be no reason to believe that similar improvements in three-dimensional momentum-integral methods cannot be found.

Present models of the boundary layer crossflow are primitive and further experimental data and research can be expected to uncover a simple crossflow velocity profile family that is adequate for calculation methods. For this reason it was thought desirable to make the technical improvements mentioned above in the von Kerczek method so as to accommodate easily detailed improvements in the crossflow model that may come about later. However, the modified surface coordinate system and the incorporation of the exact double model potential flow calculations (in lieu of the slender body theory potential flow calculation method) are of independent value and can be used with any other boundary layer calculation method. The surface coordinate system for the boundary layer calculations developed in this report has some advantages over the coordinate systems recommended by others (see, for example, Cebeci et al.[3] and Miloh and Patel[6]). The surface coordinate system used in this report is very similar to the one used by Cebeci et al.[3] but it does not have the complication of being nonorthogonal. The present surface coordinate system is superior to the Miloh and Patel[6] coordinate system because it provides a better coordinate net coverage of the hull surface for uniform spacing of the coordinate parameters.

This report is divided into six sections including the introduction. The second section describes the formulation of the boundary layer

calculation problem in terms of the momentum-integral entrainment method. The third section describes the surface coordinate system and the potential flow calculation method. The fourth section describes the numerical method for integrating the momentum-integral equations. The fifth section describes and discusses some sample computational results and the sixth section gives some concluding remarks on further developments of this three-dimensional ship boundary layer calculation method. An appendix at the end of the report gives some detailed formulas that are used in the computational algorithm.

THE BOUNDARY LAYER MOMENTUM INTEGRAL EQUATIONS

It is assumed that the ship surface is hydraulically smooth and has no abrupt changes in principal curvature anywhere on the hull. Also assumed is that the boundary layer thickness is small compared to the principal curvatures everywhere on the hull. Only the turbulent boundary layer development is considered. The length scale used is half the length, L, between the perpendiculars of the hull. The velocity scale is the steady ship speed U_∞. Henceforth, all physical quantities that are discussed will be dimensionless with respect to these scales. There is an orthogonal surface coordinate system on the hull, which has lines of constant θ running generally lengthwise along the ship and lines of constant ϕ running nearly parallel to the cross-sections of the ship. This system will be described in detail in Section 3. The coordinate perpendicular to the hull surface can be described in terms of its arc length parameter λ.

At an arbitrary point on the hull surface the potential flow velocity vector $\underline{U}$ is given by

$$\underline{U} = U_\phi \, \underline{e}_\phi + U_\theta \, \underline{e}_\theta \qquad (1)$$

where $\underline{e}_\phi$ and $\underline{e}_\theta$ are unit tangent vectors in the direction of the ϕ and θ coordinates, respectively, and $U = ||\underline{U}||$ is the magnitude of the velocity vector $\underline{U}$. The angle that the velocity vector $\underline{U}$ makes with the ϕ coordinate line is denoted by

$$\alpha = \tan^{-1}\left(\frac{U_\theta}{U_\phi}\right) \tag{2}$$

In terms of this coordinate system the momentum-integral boundary-layer equations are a special case of the equations given by Myring[7] and reproduced in the article by Reynolds and Cebeci.[8] These equations are the momentum integrals for the flow in the ϕ-direction;

$$\frac{\partial \Theta_{11}}{\partial \ell_\phi} + \frac{\partial \Theta_{12}}{\partial \ell_\theta} = \frac{1}{2} C_{f_\phi} - \Theta_{11}\left\{\frac{2}{U}\frac{\partial U}{\partial \ell_\phi} - K_\phi\right\}$$

$$- 2\,\Theta_{12}\left\{\frac{1}{U}\frac{\partial U}{\partial \ell_\theta} - K_\theta\right\} - \Theta_{22}\,K_\phi - \frac{\Delta_1}{U}\frac{\partial U_\phi}{\partial \ell_\phi}$$

$$- \frac{\Delta_2}{U}\left[\frac{\partial U_\phi}{\partial \ell_\theta} + K_\phi U_\theta - K_\theta U_\phi\right] \tag{3a}$$

and for the flow in the θ-direction

$$\frac{\partial \Theta_{21}}{\partial \ell_\phi} + \frac{\partial \Theta_{22}}{\partial \ell_\theta} = \frac{1}{2} C_{f_\theta} - K_\theta \Theta_{11} - 2\Theta_{21}\left[\frac{1}{U}\frac{\partial U}{\partial \ell_\phi} - K_\phi\right]$$

$$- \Theta_{22}\left[\frac{2}{U}\frac{\partial U}{\partial \ell_\theta} - K_\theta\right] - \frac{\Delta_1}{U}\left[\frac{\partial U_\theta}{\partial \ell_\phi} + K_\theta U_\phi\right.$$

$$\left. - K_\phi U_\theta\right] - \frac{\Delta_2}{U}\frac{\partial U_\theta}{\partial \ell_\theta} \tag{3b}$$

where ℓ_ϕ and ℓ_θ are arclength parameters in the ϕ and θ directions, respectively; K_ϕ and K_θ are the geodesic curvatures of the ϕ and θ

coordinates, respectively; Θ_{11}, Θ_{21}, Θ_{12}, Θ_{22}, Δ_1, and Δ_2 are momentum and displacement thicknesses defined, respectively, by Equations (4a,4f); and C_{f_ϕ} and C_{f_θ} are wall skin friction coefficient components in the ϕ and θ directions, respectively. The usual turbulent boundary layer assumptions of the neglect of turbulent normal stresses and the neglect of mean diffusion in directions parallel to the hull surface are incorporated in Equations (3a,3b).

The momentum and displacement thicknesses are defined by

$$\Theta_{11} = \int_0^\delta \frac{\hat{u}}{U^2} (U_\phi - \hat{u}) d\lambda \tag{4a}$$

$$\Theta_{12} = \int_0^\delta \frac{\hat{v}}{U^2} (U_\phi - \hat{u}) d\lambda \tag{4b}$$

$$\Theta_{21} = \int_0^\delta \frac{\hat{u}}{U^2} (U_\theta - \hat{v}) d\lambda \tag{4c}$$

$$\Theta_{22} = \int_0^\delta \frac{\hat{v}}{U^2} (U_\theta - \hat{v}) d\lambda \tag{4d}$$

$$\Delta_1 = \int_0^\delta \frac{U_\phi - \hat{u}}{U} d\lambda \tag{4e}$$

$$\Delta_2 = \int_0^\delta \frac{U_\theta - \hat{v}}{U} d\lambda \tag{4f}$$

where $\hat{u}$ and $\hat{v}$ are the components of the mean boundary layer velocity in the ϕ and θ directions, respectively.

In the case of streamline coordinates, in which the coordinate curves ϕ are parallel to the inviscid streamlines on the hull surface, $U_\theta \equiv 0$ and $U_\phi = U$. For this case, the momentum and displacement thicknesses of definitions (4a-4f) then will be denoted by corresponding lower case Greek letters and these definitions reduce to

$$\theta_{11} = \int_0^\delta \frac{u}{U}\left(1-\frac{u}{U}\right) d\lambda \tag{5a}$$

$$\theta_{12} = \int_0^\delta \frac{v}{U}\left(1-\frac{u}{U}\right) d\lambda \tag{5b}$$

$$\theta_{21} = -\int_0^\delta \frac{u\,v}{U^2}\, d\lambda \tag{5c}$$

$$\theta_{22} = -\int_0^\delta \left(\frac{v}{U}\right)^2 d\lambda \tag{5d}$$

$$\delta_1 = \int_0^\delta \left(1-\frac{u}{U}\right) d\lambda \tag{5e}$$

$$\delta_2 = -\int_0^\delta \frac{v}{U}\, d\lambda \tag{5f}$$

The quantity δ is some overall nominal boundary layer thickness. The relationships between the boundary layer thicknesses defined by Equations (4a-4f) and those defined by Equations (5a-5f) will be needed later and can readily be worked out. They are

$$\Theta_{11} = \theta_{11} \cos^2 \alpha - (\theta_{12}+\theta_{21}) \sin \alpha \cos \alpha + \theta_{22} \sin^2 \alpha \qquad (6a)$$

$$\Theta_{12} = (\theta_{11}-\theta_{22}) \sin \alpha \cos \alpha + \theta_{12} \cos^2 \alpha - \theta_{21} \sin^2 \alpha \qquad (6b)$$

$$\Theta_{21} = (\theta_{11}-\theta_{22}) \sin \alpha \cos \alpha + \theta_{21} \cos^2 \alpha - \theta_{12} \sin^2 \alpha \qquad (6c)$$

$$\Theta_{22} = \theta_{11} \sin^2 \alpha + (\theta_{12}+\theta_{21}) \sin \alpha \cos \alpha + \theta_{22} \cos^2 \alpha \qquad (6d)$$

$$\Delta_1 = \delta_1 \cos \alpha - \delta_2 \sin \alpha \qquad (6e)$$

$$\Delta_2 = \delta_1 \sin \alpha + \delta_2 \cos \alpha \qquad (6f)$$

The inverses of Equations (6a-6f) that relate the lower case Greek symbols θ and δ to their upper case counterparts easily can be derived.

The two momentum equations, Equations (3a,3b) are insufficient to determine the eight unknowns Θ_{11}, Θ_{12}, Θ_{21}, Θ_{22}, Δ_1, Δ_2, C_{f_θ} and C_{f_ϕ}, hence, some other integral equations and empirical information are needed. The calculation method is based on the Cumpsty and Head[9] momentum-integral method[8] which utilizes the three-dimensional entrainment equation[7]

$$\frac{1}{U}\left[\frac{\partial}{\partial \ell_\phi} (U_\phi \delta - U\Delta_1) - K_\phi (U_\phi \delta - U\Delta_1)\right.$$

$$\left. + \frac{\partial}{\partial \ell_\theta} (U_\theta \delta - U\Delta_2) - K_\theta (U_\theta \delta - U\Delta_2)\right] = F \qquad (7)$$

where F is the three-dimensional rate of entrainment function. It is assumed, in this three-dimensional boundary layer calculation method, that

F is the same function evaluated with respect to the flow components in the streamline direction as the one used for two-dimensional flows. Thus, according to Green, et al.[5]

$$F(H) \equiv 0.025\ H - 0.022 \tag{8}$$

where

$$H \equiv \frac{\delta_1}{\theta_{11}} \tag{9}$$

Furthermore, it is assumed that

$$\delta \equiv \theta_{11}(G+H) \tag{10}$$

where

$$G \equiv \frac{2\ H}{(H-1)} \tag{11}$$

Thus, the entrainment parameters, the length scale δ and the entrainment function F, are completely specified in terms of integral thicknesses defined by Equations (5a-5f). A justification for the foregoing empirical expressions can be obtained from the paper of Cumpsty and Head[9] and its antecedents.

The components C_{f_ϕ} and C_{f_θ} of the skin friction coefficient can be obtained from the skin friction coefficient C_f in the local inviscid streamline direction by the formulas

$$C_{f_\phi} = C_f(\cos\alpha - \sin\alpha \tan\beta) \tag{11a}$$

$$C_{f_\theta} = C_f(\sin\alpha + \cos\alpha \tan\beta) \tag{11b}$$

where β is the angle between the direction of the wall friction vector and the inviscid streamline. The angle β is precisely defined by

$$\tan\beta = \lim_{\lambda\to 0} \frac{v}{u} = \lim_{\lambda\to 0} \frac{\frac{\partial v}{\partial \lambda}}{\frac{\partial u}{\partial \lambda}} \tag{12}$$

where the boundary-layer velocity components u and v are in the direction of the inviscid streamline and its normal, respectively. By assuming that the component of the boundary layer flow in the inviscid streamline direction satisfies the two-dimensional velocity similarity laws, the skin friction coefficient C_f can be evaluated using a two-dimensional skin friction formula. The following skin friction formula given by Head and Patel[10] is

$$C_f = \exp(aH+b) \tag{13}$$

where $a = 0.019521 - 0.386768\ c + 0.028345\ c^2 - 0.000701\ c^3$

$b = 0.191511 - 0.83489\ c + 0.062588\ c^2 - 0.001953\ c^3$

$c = \ln R_{\theta_{11}}$

and where

$$R_{\theta_{11}} \equiv \left(\frac{U_\infty L}{2\nu}\right) U\theta_{11} \tag{14}$$

is the local streamline momentum thickness Reynolds number. Recall that U is the dimensionless (scaled by U_∞) magnitude of the local inviscid velocity

at the edge of the boundary layer and θ_{11} is the streamline component of the momentum thickness made dimensionless by the half length L of the ship.

The final empirical formulas that are used to reduce the number of unknown quantities to three, in order to match the number of differential Equations (3a,3b) and (7), are the formulas that relate the crossflow momentum and displacement thicknesses θ_{12}, θ_{21}, θ_{22}, and δ_2 to the streamline momentum and displacement thicknesses θ_{11} and δ_1. These relationships constitute the critical approximations of three-dimensional boundary layer theory in the momentum-integral framework. It is easiest to simply make crossflow and streamline flow boundary-layer profile assumptions and derive the corresponding relationships that result from the definitions (5a-5f). However it is not really necessary to proceed in this way. Basically, definitions (5a-5f) simply say that if the streamwise velocity profile u is described parametrically by parameters $[\alpha_i]_{i=1,\ldots,n}$ and the crossflow profile v is described parametrically by the parameters $[\beta_j]_{j=1,\ldots,m}$ then the boundary layer thicknesses $\theta_{k\ell}$ and δ_ℓ, k and ℓ = 1,2 are each functions of the parameters $[\alpha_i]$, $[\beta_j]$ such as $\theta_{k\ell}\ (\alpha_1,\ldots,\alpha_n;\ \beta_1,\ldots,\beta_m)$. One could determine these functions experimentally and thereby completely bypass any velocity profile assumptions.

In fact, such a scheme has already been used for the streamwise flow by using the Head entrainment method. From two-dimensional and axisymmetric flow theory, the entrainment method gives

$$\delta_1 = \delta_1(H,\theta_{11}) \tag{15a}$$

$$C_f = C_f(H,\theta_{11}) \tag{15b}$$

directly without any profile assumptions. In the most highly developed entrainment method of Green et al.,[5] a third independent parameter is added to θ_{11} and H, namely the entrainment coefficient C_E, so that

$$\delta_1 = \delta_1(H, \theta_{11}, C_E) \tag{16}$$

replaces Equation (15a). If a velocity profile is needed, then the velocity profiles of Coles[11] or Thompson[12] may be used for specified values of the momentum thickness θ_{11} and shape factor H. Sufficient experimental data for three-dimensional boundary layers are not yet available for a similar program to be conducted. It does, however, seem that the flow in the streamwise direction is sufficiently similar to two-dimensional flow that the two-dimensional data can be directly applied to this component of the boundary layer flow. However, insufficient data exist for the crossflow to make more than a crude estimate of profile shapes. There has not even been a sufficiently large collection and analysis of crossflow profiles to make a reasonable estimate of the proper parameters $[\beta_j]_{j=1,\ldots,m}$ that need to be used to approximate the crossflow. Thus, as the simplest first approximation of the crossflow profile shape, it is common practice to assume that (1) the crossflow profile scales on the same length scale δ as the streamwise profile and (2) the crossflow profile shape depends on only one or two independent parameters, one of which is the shear stress angle β. The fact that condition (12) must be satisfied at the wall introduces the angle β into the description of the crossflow profile and also dictates (as a matter of convenience) the shape assumption in the form

$$\frac{v}{U} = \left(\frac{u}{U}\right) f(\lambda) \tan \beta \tag{17a}$$

In order to satisfy condition (12) at the wall and the condition that $v = 0$ at $\lambda = \delta$ (in streamline coordinates), the function f must satisfy $f(0) = 1$ and $f(\delta) = 0$. The assumption by Mager[13] is a popular first approximation that gives

$$f(\lambda) = \left(1 - \frac{\lambda}{\delta}\right)^2 \tag{17b}$$

It should be emphasized that a profile assumption, such as Equation (17b), need not be employed at all but, at this time, lack of experimental data forces the use of such an approximation. More sophisticated profile assumptions than Equation (17b) have been made. For instance Okuno[14] assumed that

$$f(\lambda) = \left[1+C\left(\frac{\lambda}{\delta}\right)\right]\left(1-\frac{\lambda}{\delta}\right)^2 \qquad (18)$$

The parameter C in Equation (18) is governed by an additional crossflow integral equation. Okuno[14] chose the crossflow moment-of-momentum integral equation for calculating the development of the parameter C and obtained considerably better results for crossflow profile predictions than with the Mager model of Equation (17b). However, there still were certain areas on the ship hull at which the predicted crossflow velocity profiles were in serious disagreement with experiment. The areas of serious disagreement between the crossflow profiles given by Equation (18) and the experimental ones on the Okuno test model (a Series 60 block 0.70 double model) are very close to the stern on streamlines that turn upwards from the keel towards the load waterline. From Okuno's experience,[14] it seems likely that further experiments and research will eventually lead to a fairly accurate crossflow velocity profile shape function $f(\lambda)$ that involves only one or at most two extra parameters.

This report is mainly concerned with setting the proper framework for the three-dimensional momentum-integral boundary layer computational method, so it will presently be confined to the simplest of the crossflow models, namely that of Mager, Equation (17b). It is hoped that future developments and availability of sufficient experimental three-dimensional boundary layer data will warrant modifications of this method to include a more complete and accurate crossflow model along the lines of the Okuno model.

By examining definitions, Equations (5b), (5c), and (5f), it is easy to see that θ_{12}, θ_{21}, and δ_2 satisfy the relationship

$$\theta_{21} = \delta_2 + \theta_{12} \tag{19}$$

This equation can be used to eliminate one of the unknowns from the boundary layer momentum-integral equations. The Mager crossflow model, Equation (17), in conjunction with the approximation

$$\frac{u}{U} = \left(\frac{\lambda}{\delta}\right)^{(H-1)/2} \tag{20}$$

and Equation (10) for the nominal thickness δ, can be used to express the crossflow boundary layer thicknesses in terms of the streamwise momentum thickness θ_{11}, the shape parameters G and H, and the crossflow angle β by the equations

$$\theta_{21} = -\frac{2\,\theta_{11}(G+H)\,\tan\beta}{H(H+1)\,(H+2)} \equiv \theta_{11}\,\tan\beta\,\bar{f}_1(H) \tag{21a}$$

$$\theta_{12} = -\,\theta_{11}(G+H)\,\tan\beta\left[\frac{1}{H} - \frac{4}{H+1} + \frac{1}{H+2} + \frac{4}{H+3} - \frac{2}{H+5}\right] \equiv \theta_{11}\,\tan\beta\,\bar{f}_2(H) \tag{21b}$$

$$\theta_{22} = -\,\theta_{11}(G+H)\,\tan^2\beta\left[\frac{1}{H} - \frac{4}{H+1} + \frac{6}{H+2} - \frac{4}{H+3} + \frac{1}{H+4}\right] \equiv \theta_{11}\,\tan^2\beta\,\bar{f}_3(H) \tag{21c}$$

$$\delta_2 = -\,\theta_{11}(G+H)\,\tan\beta\left[\frac{2}{H-1} - \frac{4}{H+3} + \frac{2}{H+5}\right] \equiv \theta_{11}\,\tan\beta\,\bar{f}_4(H) \tag{21d}$$

Thus Equations (8) through (11), (13), (17), (19), and (21), together with the transformation Equations (6a-6f), can be used to reduce the total number of unknown quantities to three. A convenient set of unknown quantities, that are integrated in the (ϕ,θ) coordinate system by Equations (3) and (7) are the streamwise momentum thickness θ_{11}, the shape factor H, and the tangent of the wall crossflow angle $t = \tan\beta$. The details of the final forms of Equations (3) and (7) in terms of these variables are given in the appendix.

THE SHIP SURFACE COORDINATE SYSTEM

The hull surface coordinate system that is used in the boundary layer calculation method described in the previous section stems directly from the hull surface representation of von Kerczek and Tuck.[15] This hull surface representation utilizes conformal mapping onto a unit circle of the cross sections of the hull and polynomial interpolation along the length of the hull of the individual mapping coefficients. Let s be the longitudinal coordinate, x the lateral coordinate, and y the vertical coordinate of the ship hull. These coordinates are made dimensionless by the half length L so that the bow and stern perpendiculars lie at $s = \mp 1$, respectively. The load water-line is located at $y = 0$ and the keel at midships is located at $y = -D$.

The hull surface representation of von Kerczek and Tuck[15] results in a parametric surface equation of the form

$$z = x + iy = \sum_{n=1}^{N} \sum_{m=1}^{M} A_{mn} \, e^{i(3-2n)\theta} s^{m-1} \tag{22}$$

where the matrix (A_{mn}) of coefficients specifies the hull form and is computed from a set of defining hull offsets by an algorithm given by von Kerczek and Tuck.[15]

The surface coordinate system used in the boundary layer equations consists of the θ = constant lines, obtained from Equation (22) and their orthogonal trajectories, here denoted by ϕ = constant lines. It is not necessary to specify the variable ϕ since the arclength along the ϕ = constant lines will be used directly.

Equation (22) can be written in real form as

$$x = x(s,\theta) = \sum_{n=1}^{N} \sum_{m=1}^{M} A_{mn} \, s^{m-1} \cos(3-2n)\theta \tag{23a}$$

$$y = y(s,\theta) = \sum_{n=1}^{N} \sum_{m=1}^{M} A_{mn}\, s^{m-1} \sin(3-2n)\theta \qquad (23b)$$

and, in the vector form,

$$\underline{r} = \underline{r}(s,\theta) = x(s,\theta)\underline{i} + y(s,\theta)\underline{j} + s\underline{k} \qquad (24)$$

where $\underline{r}$ is the vector from the origin of the (x,y,s) coordinate system to a point on the hull surface, and $(\underline{i},\underline{j},\underline{k})$ are unit tangent vectors to the (x,y,s) coordinates, respectively.

The surface coordinate lines θ = constant, run along the length of the hull surface, and the coordinate lines ϕ = constant, are nearly parallel to the hull cross-sections. The arclength increments along the ϕ and θ coordinates are $d\ell_\phi$ and $d\ell_\theta$, respectively, and are given by

$$d\ell_\phi = (d\underline{r}\cdot d\underline{r})^{1/2}_{\theta=\text{constant}}$$

$$= \left[\left(\frac{\partial x}{\partial s}\right)^2 + \left(\frac{\partial y}{\partial s}\right)^2 + 1\right]^{1/2} ds \qquad (25a)$$

and

$$d\ell_\theta = (d\underline{r}\cdot d\underline{r})^{1/2}_{\phi=\text{constant}}$$

$$= \left[\left(\frac{\partial x}{\partial \theta} + \frac{\partial x}{\partial s}\frac{ds}{d\theta}\bigg|_\phi\right)^2 + \left(\frac{\partial y}{\partial \theta} + \frac{\partial y}{\partial s}\frac{ds}{d\theta}\bigg|_\phi\right)^2 + \left(\frac{ds}{d\theta}\bigg|_\phi\right)^2\right]^{1/2} d\theta \qquad (25b)$$

where $(ds/d\theta|_\phi)$ denotes the evaluation of the derivative $ds/d\theta$ along the ϕ = constant line.

Let $\underline{e}_\phi$, $\underline{e}_\theta$, and $\underline{e}_n$ be unit tangent vectors to the ϕ, θ, and the hull surface normal coordinates, respectively. Then $\underline{e}_\theta$ and $\underline{e}_n$ are easily computed using Equation (24) by

$$\underline{e}_\phi = \frac{\dfrac{\partial \underline{r}}{\partial s}}{\left|\left|\dfrac{\partial \underline{r}}{\partial s}\right|\right|} \tag{26}$$

$$\underline{e}_n = \frac{\left(\dfrac{\partial \underline{r}}{\partial s} \times \dfrac{\partial \underline{r}}{\partial \theta}\right)}{\left|\left|\dfrac{\partial \underline{r}}{\partial s} \times \dfrac{\partial \underline{r}}{\partial \theta}\right|\right|} \tag{27}$$

where $||\cdot||$ denotes the length of the vector. The requirement that the ϕ and θ coordinates be orthogonal imposes the condition that

$$\underline{e}_\theta = \underline{e}_n \times \underline{e}_\phi \tag{28}$$

The increment of arc along the curve ϕ = constant, $d\underline{r}|_\phi$, can be written as

$$d\underline{r}\Big|_\phi = \left(\frac{\partial \underline{r}}{\partial \theta} + \frac{\partial \underline{r}}{\partial s}\frac{ds}{d\theta}\right) d\theta \tag{29}$$

and by virtue of orthogonality

$$\underline{e}_\phi \cdot d\underline{r}\Big|_\phi = 0 \tag{30}$$

The derivative $(ds/d\theta)_\phi$ can be obtained from Equation (30) by

$$\frac{ds}{d\theta}\Big|_\phi = -\frac{\left(\dfrac{\partial x}{\partial \theta}\dfrac{\partial x}{\partial s} + \dfrac{\partial y}{\partial \theta}\dfrac{\partial y}{\partial s}\right)}{\left[\left(\dfrac{\partial x}{\partial \theta}\right)^2 + \left(\dfrac{\partial y}{\partial \theta}\right)^2 + 1\right]} \tag{31}$$

The geodesic curvature terms K_ϕ and K_θ are defined, respectively, by

$$K_\phi = \underline{e}_\phi \cdot \frac{d\underline{e}_\theta}{d\ell_\phi} \tag{32a}$$

$$K_\theta = \underline{e}_\theta \cdot \frac{d\underline{e}_\phi}{d\ell_\theta} \tag{32b}$$

The derivatives in Equations (32a,32b) can be evaluated by converting them to derivatives with respect to s and θ using Equations (25a,25b), respectively.

Miloh and Patel[6] recommended the use of the orthogonal surface coordinate system that consists of the cross-section curves and their orthogonal trajectories on the hull surface. In terms of the surface Equation (23) the cross-section curves are given by s = constant. Thus, if $\underline{e}$, in this case, is the unit tangent vector to the cross-section profile, the orthogonal trajectories of the cross-sections can be computed by integrating the differential equation

$$\underline{e} \cdot d\underline{r} = 0 \tag{33}$$

which, in expanded form, and making use of Equation (29), reads

$$\frac{d\theta}{ds} = - \frac{\underline{e} \cdot \frac{\partial \underline{r}}{\partial s}}{\left(\underline{e} \cdot \frac{\partial \underline{r}}{\partial \theta} \right)} \tag{34}$$

Examples of hull surface coordinate grids for the (ϕ,θ) system described earlier and the cross-section system of Equation (34) are given in the section on Computational Results and Discussion.

The potential flow velocity on the surface of the hull was obtained by using the computer program of Chang.[16] This program solves the double-model Neumann problem by distributing a layer of doublets on the hull surface and numerically solving the resulting integral equation by a panel method. The main advantage of using a doublet distribution, rather than a source distribution as in the Hess-Smith method,[17] is that the surface potential is obtained directly as the solution of the integral equation.

The hull surface representation, Equation (23), is used to generate the input for the potential flow program of Chang.[16] A uniform rectangular distribution of points in the (ϕ,θ) plane determines a set of curved quadrilateral elements covering the hull surface. These curved quadrilateral elements are approximated by plane quadrilateral elements and then used as input into the Chang program. The results of the potential flow calculation are values of the surface velocity potential at the geometric midpoints of the plane quadrilateral elements. These values of the surface velocity potential are then assumed to be accurate values of the exact surface velocity potential at the points of the hull surface that correspond to the geometric centers of the rectangular elements in the (ϕ,θ) plane. The value of the surface velocity at each point is obtained by numerical differentiation of the surface velocity potential. The values of the potential are first interpolated along ϕ = constant curves by a periodic cubic spline.[18] This interpolation yields accurate values of the surface velocity potential at arbitrary locations on the θ = constant curves. Then the values of the surface velocity potential are interpolated along θ = constant curves by another cubic spline. The surface velocities and the derivatives of the surface velocities that are required in Equations (3) and (7) are obtained, respectively, by differentiating the cubic spline, evaluating the result, which gives the velocities, and then refitting the velocities with cubic splines and differentiating the second set of splines. This "spline-on-spline" procedure[18] seems to be one of the best ways of obtaining two derivatives of a numerically defined function.

NUMERICAL ANALYSIS

The two momentum integral Equations (3a,3b), together with the entrainment Equation (7), can be written completely in the form

$$D(W(\phi,\theta))\,\frac{\partial W}{\partial \ell_\phi} + B(W(\phi,\theta))\,\frac{\partial W}{\partial \ell_\theta} = C(W) \tag{35}$$

where the vector W is given by

$$W = \begin{pmatrix} W_1 \\ W_2 \\ W_3 \end{pmatrix} = \begin{pmatrix} \theta_{11} \\ t \\ H \end{pmatrix} \tag{36}$$

From Equations (50) and (55) in the appendix, the coefficient matrices are defined as follows:

$$D(W) = (D_{ij}) = \begin{pmatrix} g_{11} & \theta_{11}\dfrac{\partial g_{11}}{\partial t} & \theta_{11}\dfrac{\partial g_{11}}{\partial H} \\ g_{21} & \theta_{11}\dfrac{\partial g_{21}}{\partial t} & \theta_{11}\dfrac{\partial g_{21}}{\partial H} \\ h_{11} & \theta_{11}\dfrac{\partial h_{11}}{\partial t} & \theta_{11}\dfrac{\partial h_{11}}{\partial H} \end{pmatrix} \tag{37a}$$

$$B(W) = (B_{ij}) = \begin{pmatrix} g_{12} & \theta_{11}\dfrac{\partial g_{12}}{\partial t} & \theta_{11}\dfrac{\partial g_{12}}{\partial H} \\ g_{22} & \theta_{11}\dfrac{\partial g_{22}}{\partial t} & \theta_{11}\dfrac{\partial g_{22}}{\partial H} \\ h_{22} & \theta_{11}\dfrac{\partial h_{22}}{\partial t} & \theta_{11}\dfrac{\partial h_{22}}{\partial H} \end{pmatrix} \tag{37b}$$

and

$$C(W) = (C_i) = \begin{pmatrix} C_1 \\ C_2 \\ C_3 \end{pmatrix} \tag{37c}$$

where

$$C_1 = \frac{1}{2} C_{f_\phi} - \frac{2\,\theta_{11}\, g_{11}}{U} \frac{\partial U}{\partial \ell_\phi} - \frac{2\,\theta_{11}\, g_{12}}{U} \frac{\partial U}{\partial \ell_\theta}$$

$$- \frac{\Delta_1}{U} \frac{\partial u_\phi}{\partial \ell_\phi} - \frac{\Delta_2}{U} \frac{\partial u_\phi}{\partial \ell_\theta} + \theta_{11}\, K_\theta (g_{12}+g_{21}+h_1 \sin\alpha) \tag{37d}$$

$$+ \theta_{11}\, K_\phi (g_{11}-g_{22}-h_2 \sin\alpha)$$

$$C_2 = \frac{1}{2} C_{f_\theta} - \frac{2\,\theta_{11}}{U} \left(g_{21} \frac{\partial U}{\partial \ell_\phi} + g_{22} \frac{\partial U}{\partial \ell_\theta} \right)$$

$$- \frac{1}{U} \left(\Delta_1 \frac{\partial u_\theta}{\partial \ell_\phi} + \Delta_2 \frac{\partial u_\theta}{\partial \ell_\theta} \right) + \theta_{11}\, K_\phi (g_{12}+g_{21}+h_2 \cos\alpha) \tag{37e}$$

$$+ \theta_{11}\, K_\theta (g_{22}-g_{11}-h_1 \cos\alpha)$$

and

$$C_3 = F(H) - \frac{1}{U} \left(T \frac{\partial U}{\partial \ell_\phi} - S \frac{\partial U}{\partial \ell_\theta} \right) + TK_\phi + SK_\theta \tag{37f}$$

The variables in Equation (35) and auxiliary formulas of Equation (37) are defined in terms of the principal unknown momentum and displacement thicknesses Θ_{11}, Θ_{12}, Θ_{21}, Θ_{22}, Δ_1, and Δ_2 in the appendix. It is assumed that the values of W are known at a given station $\phi = \phi_0$ for all values of θ and that the boundary layer is to be computed between ϕ_0 and a final station ϕ_f downstream of ϕ_0. Because of symmetry, it is only necessary to solve Equation (35) between $\theta = -\pi/2$ and $\theta = 0$. An $(N+1) \times (M+1)$ grid with spacing $\Delta\phi$ and $\Delta\theta$, respectively, is superimposed on the region $[(\phi,\theta)|\phi_0 \leq \phi \leq \phi_f, -\pi/2 \leq \theta \leq 0]$. For simplicity of notation, W^{ij} will denote $W(\phi_0+i\Delta\phi_0, j\Delta\theta)$. For $i = 0, 1,\ldots,N$ and $j = 0, 1,\ldots,M$. Also D^{ij}, B^{ij}, and C^{ij} will denote the values of the matrices B, C, and D, respectively, at the point $(\phi_0+i\Delta\phi, j\Delta\theta)$.

Equation (35) is hyperbolic if there is a nonzero crossflow. The three characteristics at a point (ϕ,θ) lie between the angles α and $\alpha + \beta$; the equation is parabolic at a point if β is zero, as the characteristics have the same tangent or, equivalently, the same direction. Along a line of flow symmetry, such as at the keel or at the waterline on a double model, the crossflow is zero and the governing Equation (35) is parabolic. Consequently, in the present case of the double hull models, Equation (35) is a mixed equation, that is hyperbolic and parabolic at different points of the region of integration unless the crossflow is everywhere zero. In this latter case, Equation (35) reduces to parabolic form. A solution method which is applicable to both parabolic and hyperbolic equations must, therefore, be used to solve Equation (35) for double hull models or hulls for which the crossflow is zero or very small everywhere.

The O'Brien et al.,[19] implicit finite difference scheme is used to solve Equation (35). It is a stable scheme for any positive grid spacing ratio $r = \Delta\theta/\Delta\phi$ and is applicable to both hyperbolic and parabolic equations. It consists of a one-step forward difference in the ϕ-direction and a central difference at the $i + 1$ step in the θ-direction. In this numerical integration scheme, Equation (35) is approximated by the equation

$$\frac{D^{ij}}{h_\phi}\left(\frac{W^{i+1j}-W^{ij}}{\Delta\phi}\right) + \frac{B^{ij}}{h_\theta}\left(\frac{W^{i+1j+1}-W^{i+1j-1}}{2\Delta\theta}\right) = C^{ij} \qquad (38)$$

where the metrics h_ϕ and h_θ (defined by $\ell_\phi = h_\phi d\phi$ and $\ell_\theta = h_\theta d\theta$) are evaluated at the point $(\phi_0 + i\Delta\phi, j\Delta\theta)$. Rearranging the terms of Equation (38) yields the equation

$$- \bar{B}^{ij} W^{i+1\ j-1} + D^{ij} W^{i+1j} + \bar{B}^{ij} W^{i+1\ j+1}$$

$$= \bar{C}^{ij} = D^{ij} W^{ij} + h_\phi \Delta\phi\, C^{ij} \tag{39a}$$

where

$$\bar{B}^{ij} = \left(\frac{h_\phi}{2rh_\theta}\right) B^{ij} \tag{39b}$$

The values of W^{oj} for $j = 0, 1, \ldots, M$ are specified initial conditions; they may be obtained from experimental data. Along the symmetry lines $j = 0$ $(\theta = 0)$ and $j = M$ $\left(\theta = -\frac{\pi}{2}\right)$, the crossflow angle β is zero, so that $W_2 = t = 0$, the equation $W_2 \equiv 0$ replaces the second momentum Equation (36) along the two lines of symmetry, the load waterline and the keel. Moreover, $\alpha = 0$ on these lines, so that g_{12}, g_{21}, g_{22}, h_2, h_{22}, S, C_{f_θ}, Δ_2, and $\frac{\partial h_{22}}{\partial H}$ are identically zero. Thus, along the symmetry lines, the momentum integral Equation (3a) reduces to the equation

$$\frac{\partial \theta_{11}}{\partial \ell_\phi} + \theta_{11} \frac{\partial g_{12}}{\partial t} \frac{\partial t}{\partial \ell_\theta} = \frac{1}{2} C_{f_\phi} + \theta_{11} \left(K_\phi - \frac{H+2}{U} \frac{\partial U}{\partial \ell_\phi}\right) \tag{40}$$

and the auxiliary Equation (7) reduces to the equation

$$G \frac{\partial \theta_{11}}{\partial \ell_\phi} + \theta_{11} \frac{dG}{dH} \frac{\partial H}{\partial \ell_\phi} + \theta_{11} \frac{\partial h_{22}}{\partial t} \frac{\partial t}{\partial \ell_\theta} = F(H) - \theta_{11} G \left(\frac{1}{U} \frac{\partial U}{\partial \ell_\phi} - K_\phi\right) \tag{41}$$

(See the appendix for details). The system of Equation (35) can be used also to represent Equations (40) and (41) together with $t \equiv 0$, if the coefficient matrices B, C, and D are modified to the following:

$$D(W) = \begin{pmatrix} 1 & 0 & 0 \\ 0 & 1 & 0 \\ 0 & 0 & \theta_{11} \frac{dG}{dH} \end{pmatrix} \tag{42a}$$

$$B(W) = \begin{pmatrix} 0 & \theta_{11} \frac{\partial g_{12}}{\partial t} & 0 \\ 0 & 0 & 0 \\ 0 & \theta_{11} \frac{\partial h_{22}}{\partial t} & 0 \end{pmatrix} \tag{42b}$$

and

$$C(W) = \begin{pmatrix} \frac{1}{2} C_{f_\phi} + \theta_{11} \left(K_\phi - \frac{H+2}{U} \frac{\partial U}{\partial \ell_\phi} \right) \\ 0 \\ F(H) - \theta_{11} G \left(\frac{1}{U} \frac{\partial U}{\partial \ell_\phi} - K_\phi \right) \end{pmatrix} \tag{42c}$$

The crossflow angle is asymmetric with respect to $\theta = 0$, so t is also asymmetric with respect to this line. Accordingly, the central difference approximation for $\partial t / \partial \ell_\theta$ on the $\theta = 0$ line is

$$\frac{t^{i1} - (-t^{i1})}{2h_\theta \Delta\theta} = \frac{t^{i1}}{h_\theta \Delta\theta} \tag{43}$$

The zero crossflow finite difference formula analogous to Equation (38) is

$$\frac{D^{i0}}{h_\phi}\left(\frac{W^{i+1\ 0} - W^{i0}}{\Delta\phi}\right) + \frac{B^{i0}}{h_\theta}\frac{W^{i+1\ 1}}{\Delta\theta} = C^{i0} \tag{44}$$

After rearranging the terms of Equation (44), one obtains the equation

$$D^{i0}\ W^{i+1\ 0} + \bar{B}^{i0}\ W^{i+1\ 1} = \bar{C}^{i0} \tag{45a}$$

where

$$\bar{B}^{i0} = \frac{h_\phi}{r h_\theta}\ B^{i0} \tag{45b}$$

A similar argument at the symmetry plane $\theta = -\pi/2$ yields the finite difference equation

$$-\bar{B}^{iM}\ W^{i+1\ M-1} + D^{iM}\ W^{i+1\ M} = \bar{C}^{iM} \tag{46a}$$

where

$$\bar{B}^{iM} = \frac{h_\phi}{r h_\theta}\ B^{iM} \tag{46b}$$

The finite difference Equations (35), (45), and (46) form a linear system of algebraic equations for the unknowns $W^{i+1\ j}$ where $i = 0,1,\ldots,N$ and $j = 0,1,\ldots,M$.

Let matrix D be defined by

$$
D = \begin{pmatrix}
D^{i0} & B^{i0} & 0 & 0 & \cdots & & & \\
-\bar{B}^{i1} & D^{i1} & \bar{B}^{i1} & 0 & 0 & \cdots & & \\
0 & \bar{B}^{i2} & D^{i2} & \bar{B}^{i2} & 0 & 0 & \cdots & \\
\cdots & \cdots & \cdots & \cdots & \cdots & \cdots & \cdots & \\
\cdots 0 & 0 & -\bar{B}^{ij} & D^{ij} & & \bar{B}^{ij} & 0 & \cdots \\
\cdots 0 & 0 & -\bar{B}^{ij+1} & & D^{ij+1} & \bar{B}^{ij+1} & 0 & 0 \cdots \\
\cdots & \cdots & \cdots & \cdots & \cdots & \cdots & \cdots &
\end{pmatrix} \tag{47}
$$

The system of linear equations then can be written in the form

$$
D\underline{X} = C \tag{48a}
$$

where $X = (x_\mu)^t$ and $C = (c_\mu)$ for $\mu = 1,\ldots,3(M+1)$, where the components x_μ of the vector $\underline{X}$ are defined by

$$
x_{3k+\kappa} = w_\kappa^{i+1\ k} \tag{48b}
$$

where $\kappa = 1,2,3$ and the components c_μ of the vector C are defined by

$$
c_{3k+\kappa} = \bar{C}_\kappa^{ik} \tag{48c}
$$

Gaussian reduction is used to solve Equation (48). The 3×3 submatrices of D have been inverted explicitly so that the Gaussian reduction of Equation (48) is very fast on the computer. Back substitution is used to obtain the vector $\underline{X}$.

COMPUTATIONAL RESULTS AND DISCUSSION

Some sample computational results of the boundary layer on two double ship models are presented in this section. The first sample computational

result is the boundary layer on the Lucy Ashton model for which experimental boundary layer data are given by Joubert and Matheson[20] and which von Kerczek[1] computed using the small crossflow approximation. The second sample computational result described below is the boundary layer development on the Swedish SSPA Model 720 for which boundary layer experimental data and calculations are provided by Larsson.[21]

It is first necessary to describe some details of the calculation of the surface coordinate system before embarking on a description of the results of the boundary layer calculation. There are many different surface coordinate systems that one can use for three-dimensional boundary layer calculation methods. The most prevalent coordinate systems used for ship boundary layers are the streamline coordinate system and the coordinate system made up of the cross-sectional curves and their orthogonal trajectories on the hull surface;[6] henceforth referred to simply as the cross-section system. The streamline coordinate system[1] has the advantage of yielding the simplest form of the boundary layer equations, but it may be difficult and costly to generate this system when flows about a ship hull at nonzero Froude number are considered. Thus it is worthwhile to consider coordinate systems that only depend on the ship hull geometry and not on the inviscid flow.

Figure 1 shows a sample of the cross-section coordinate system recommended by Miloh and Patel[6] on the Swedish SSPA Model 720. The calculation of the network of coordinate lines shown in Figure 1 is described in the previous section of this report, Calculation of the Surface Coordinate System and Potential Flow. The main feature of the cross-sectional coordinate system that has been found to be objectionable is that the lengthwise running coordinate lines seem to diverge on certain portions of the hull (at keel near the bow and stern) where the opposite, i.e., convergence of these lines, is desirable. Another, minor, annoyance of this coordinate system is that it is difficult to find the set of starting values at any particular station for the coordinate lines along the length (the orthogonal trajectories of the cross-sections) that will result in a suitable surface coordinate grid. Such a grid should not have large grid intervals or

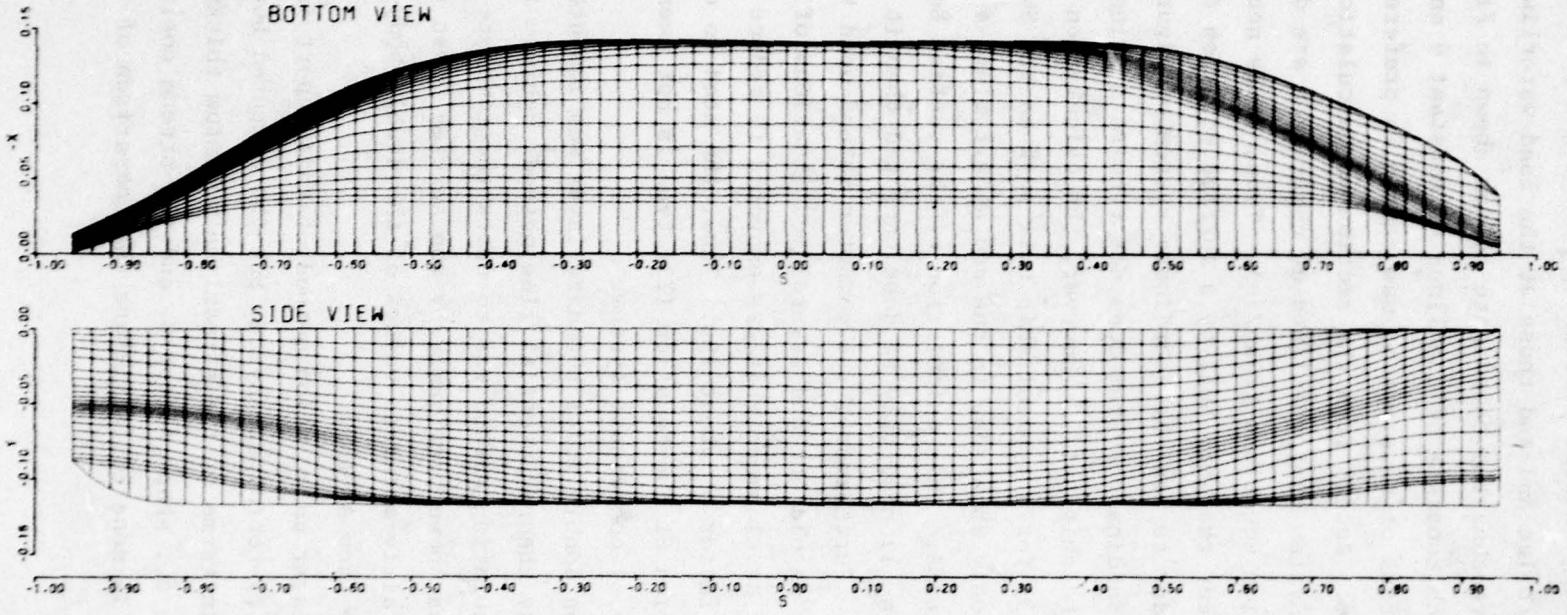

Figure 1 - The Bottom and Side Views of the Coordinate Net Consisting of the Cross-Sections and their Orthogonal Trajectories, as Recommended by Miloh and Patel,[6] on the SSPA-720 Model

excessive grid crowding on some portion of the hull (for instance note the trajectories on the bilge and and those at the load waterline near the stern). For these reasons the coordinate system shown in Figure 2 for SSPA Model 720, which consists of the lines of constant θ and their orthogonal trajectories of constant ϕ, was chosen in preference to the cross-section system. Recall from the section on Calculation of the Surface Coordinate System that the lines of constant θ are defined by the surface representation Equations (23a,23b). Thus, it is necessary to always first represent the ship hull by a surface equation of the type of Equation (23) in order to use the coordinate system of Figure 2, whereas the cross-section coordinate system does not require a prior analytical representation of the ship hull.[6] However, the calculation of the ship surface Equation (23) for a typical ship hull such as the Swedish SSPA Model 720 requires only about one to one and a half minutes of CDC 6700 computer execution time. This calculation of the surface Equation (23) (i.e., the matrix (A_{mn})) need only be done once and then it is available for several other uses. Furthermore, the computer method used to calculate the matrix (A_{mn}) is an old one and several modifications of this method are presently under development that are expected to reduce the computational time by a factor of about 100. Thus, the need to calculate the surface representation of the Equation (23) type is not seen as a disadvantage of the (θ,ϕ)-coordinate system.

The Lucy Ashton double model boundary layer was computed using the earlier slender body theory potential flow method[1] because the first test of the present calculation method was to check the complete crossflow formulation. It was shown previously by von Kerczek[1] that the slender body theory gives fairly accurate values of the double-body pressure distribution on the Lucy Ashton.

The boundary layer calculation method of this report is implemented in terms of the (θ,ϕ)-coordinate system but the computed boundary layer results are given in terms of the streamline momentum thickness θ_{11}, displacement thickness δ_1, shape factor H, and the stream coefficient of skin friction C_f. This is done to facilitate the comparison of the present

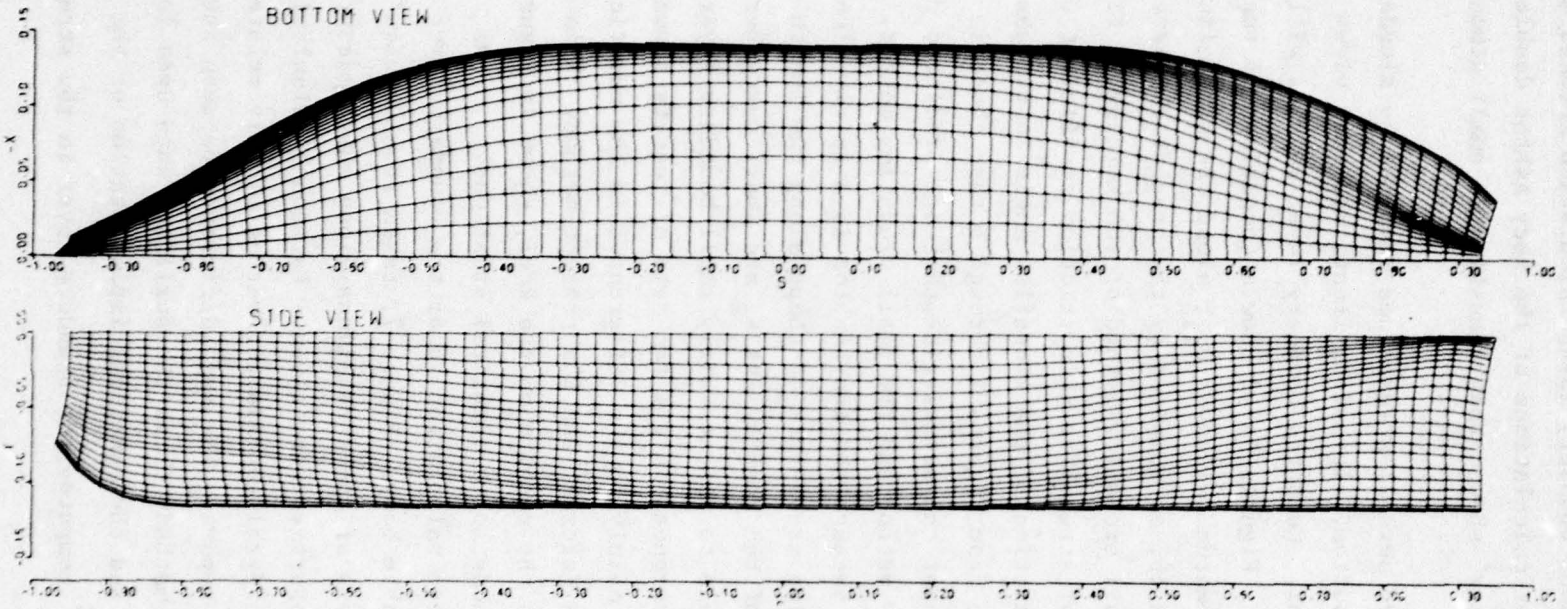

Figure 2 - The Bottom and Side Views of the (ϕ,θ) Coordinate Net on the SSPA-720 Model

results with previous boundary layer calculation methods and experiments.[1,21] Earlier calculations of the Lucy Ashton double body boundary layer by von Kerczek[1] showed that crossflow is small almost everywhere on the hull.

Figure 3 shows several streamlines computed by slender body potential flow theory. In bottom, elevation, front, and rear views on the Lucy Ashton double model. Computed boundary layer results will be shown along these streamlines. Figures 4a-4d show a comparison of the distribution of the streamline momentum thickness θ_{11}, along the streamlines 1, 6, 10, and 13 shown in Figure 3b, as computed by the present complete crossflow method and the small crossflow method of von Kerczek.[1] Figures 5a-5d show the distribution of streamline skin friction coefficient C_f and Figures 6a-6c show the distribution of the crossflow angle in radians along these same streamlines. Note from Figures 3 through 6 that there is little difference in the boundary layer characteristics that are predicted by the present complete crossflow method and the small crossflow method. This is not an unexpected result because the Lucy Ashton is a fairly slender hull with very slowly changing cross-section shape along the length of the ship. Hence the values of the coefficient K_2 are small everywhere along the hull and it is reasonable to expect fairly small boundary layer crossflow effects. The differences in the two sets of results shown in Figures 3 through 6 are due mainly to the differences in the numerical integration method used by von Kerczek[1] and the present method. This is indicated by the differences in the results on the keel, shown in Figures 4d and 5d, where the two methods solve identical equations.

The second test calculation is of the boundary layer on the Swedish SSPA Model 720 double body. Figure 7, taken from Larsson's report,[21] shows front and rear views of the streamlines along which measured and computed boundary layer properties were given. Larsson's calculation method starts from a momentum-integral-entrainment method closely related to the one described in this report. The main difference between these two boundary layer calculation methods is in the auxiliary data used for the crossflow velocity profiles and the numerical implementation of the methods. Larsson's method[21] computes the boundary layer in the streamline surface

Figure 3 - Streamlines on the Lucy Ashton Model

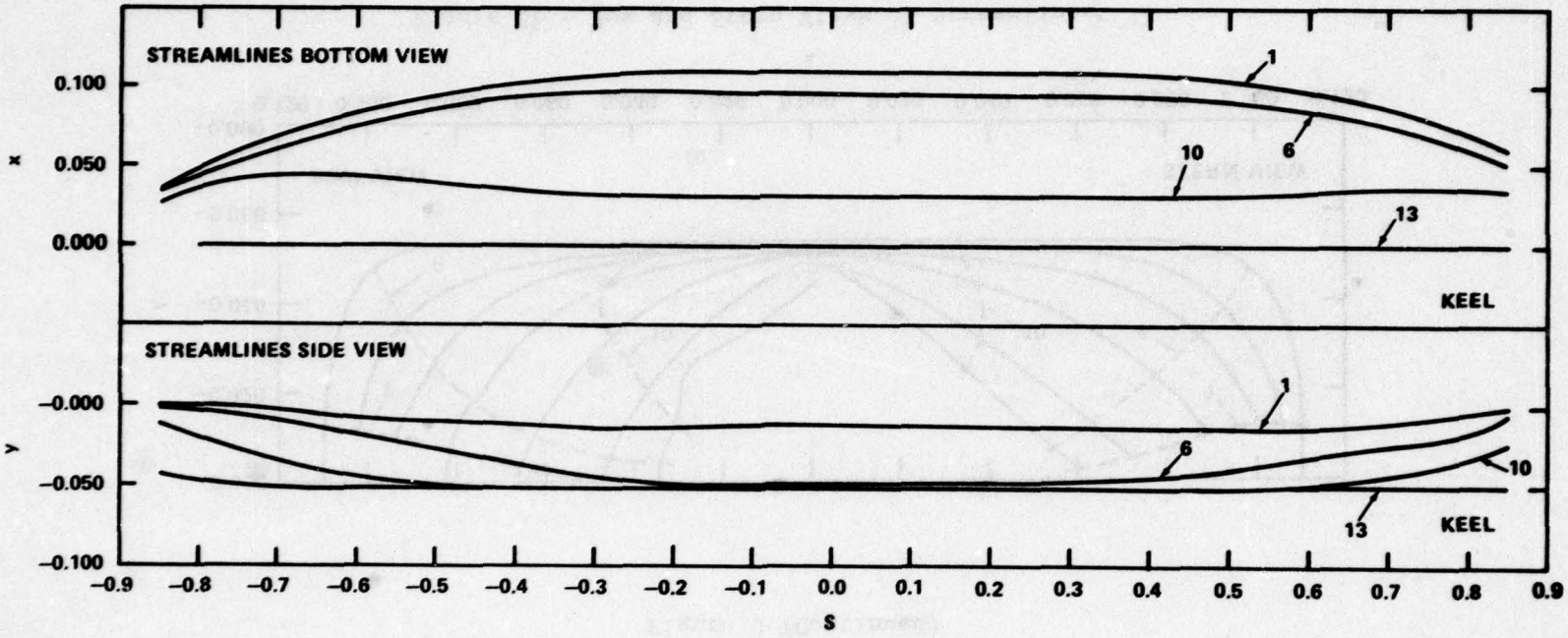

Figure 3a - Bottom and Side Views of Streamlines

Figure 3 (Continued)

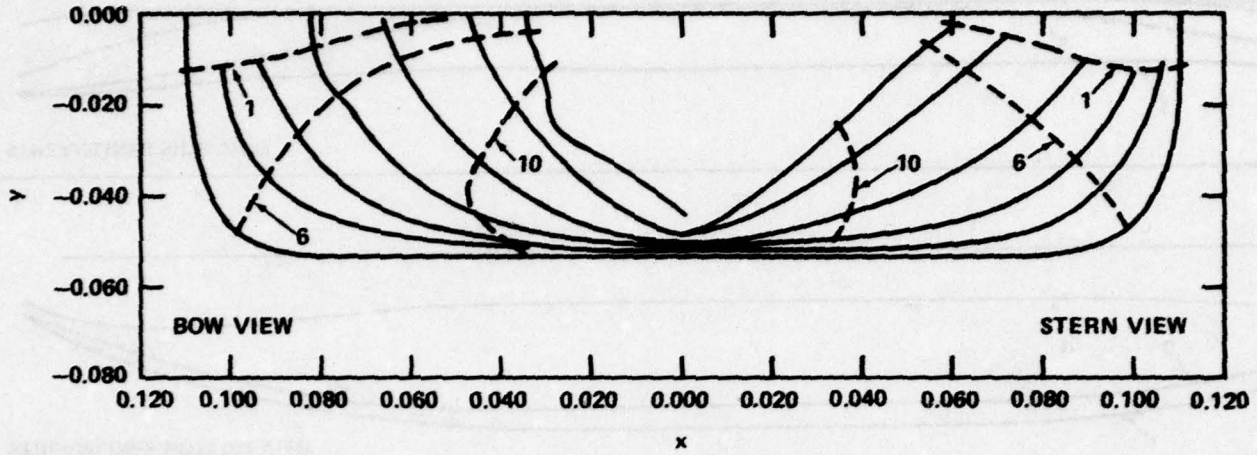

Figure 3b - Bow and Stern Views of Streamlines

Figure 4 - Streamline Momentum Thickness versus Axial Distance for Flow Along Streamlines of the Lucy Ashton

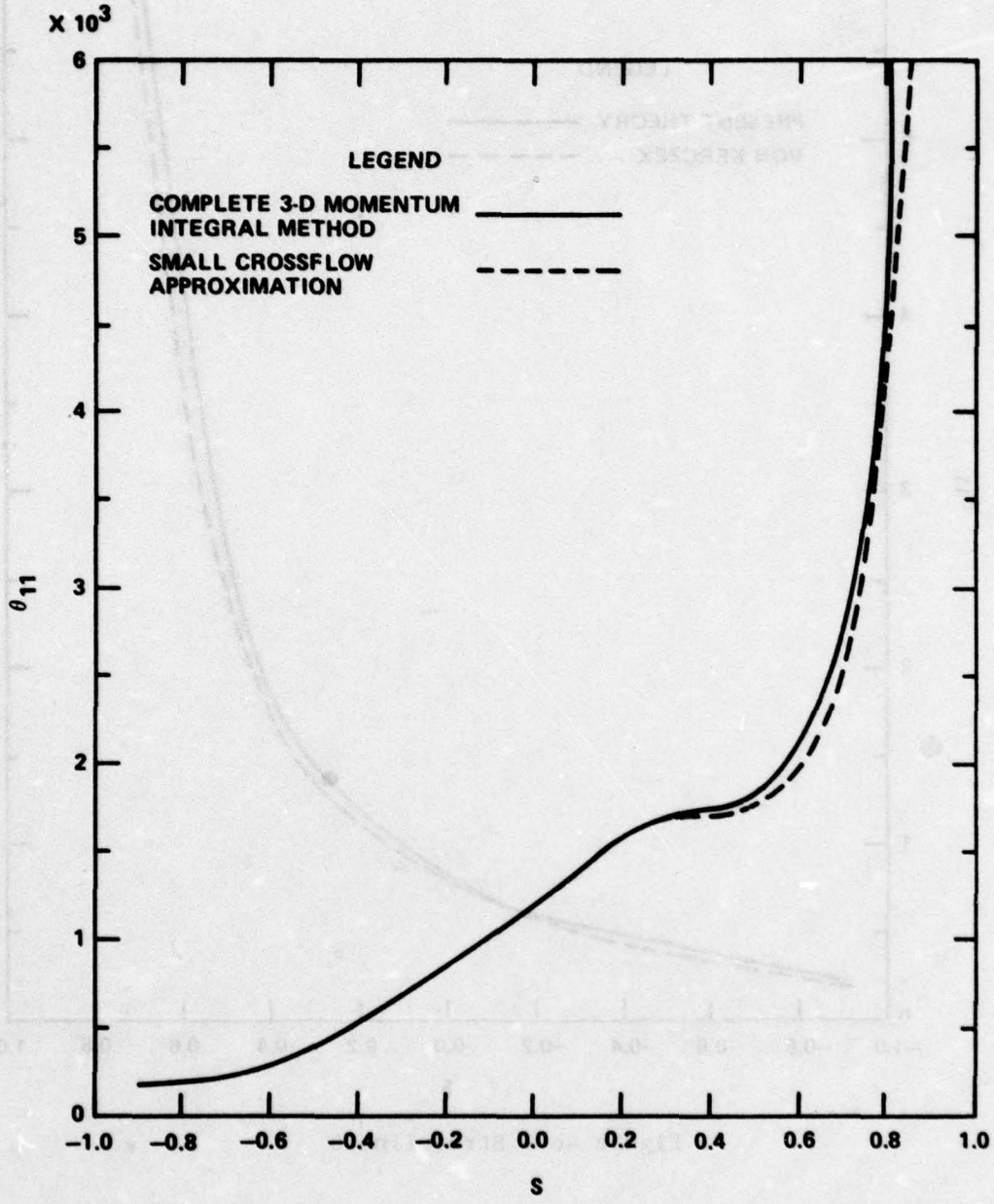

Figure 4a - Streamline 1

Figure 4 (Continued)

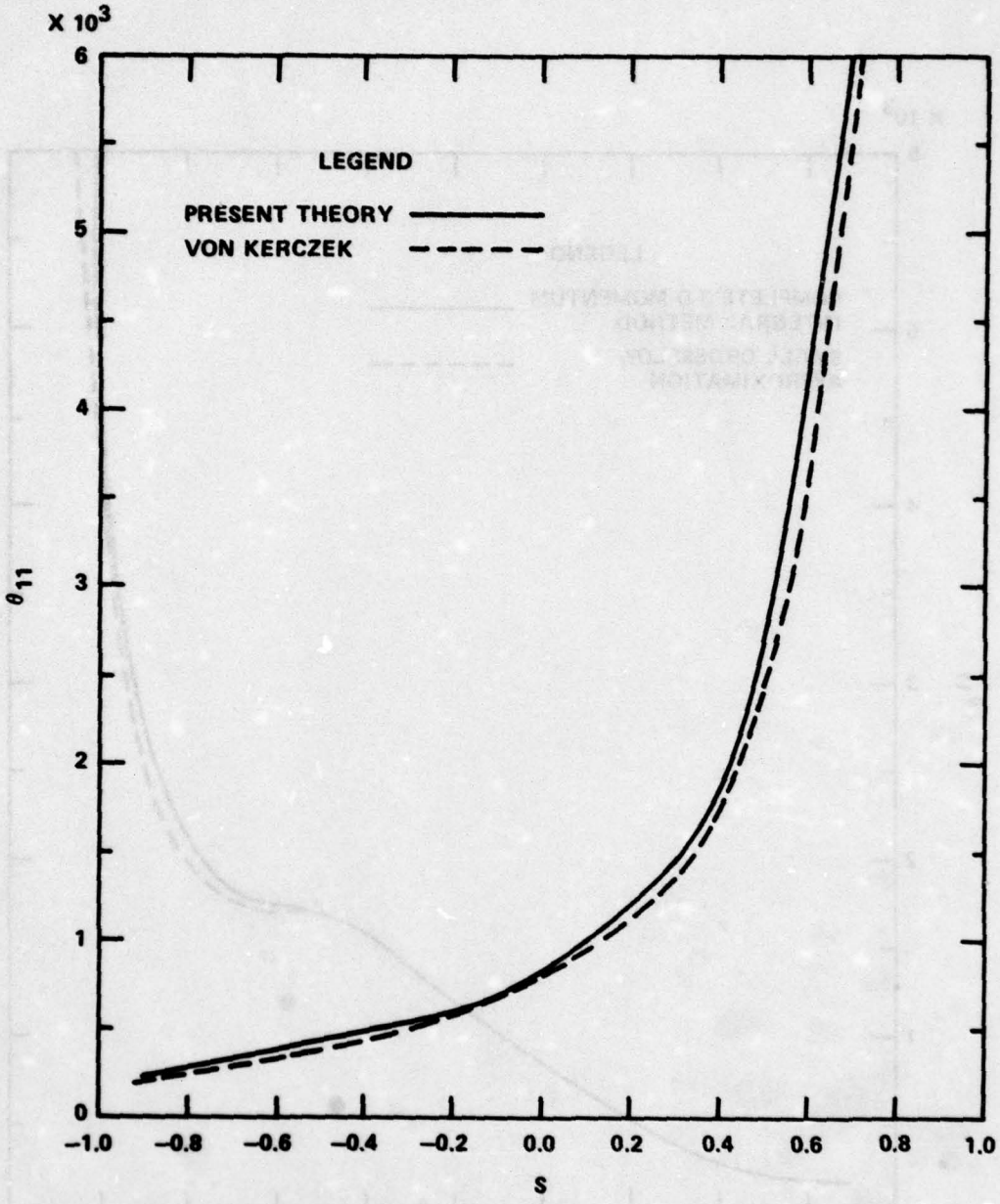

Figure 4b - Streamline 6

Figure 4 (Continued)

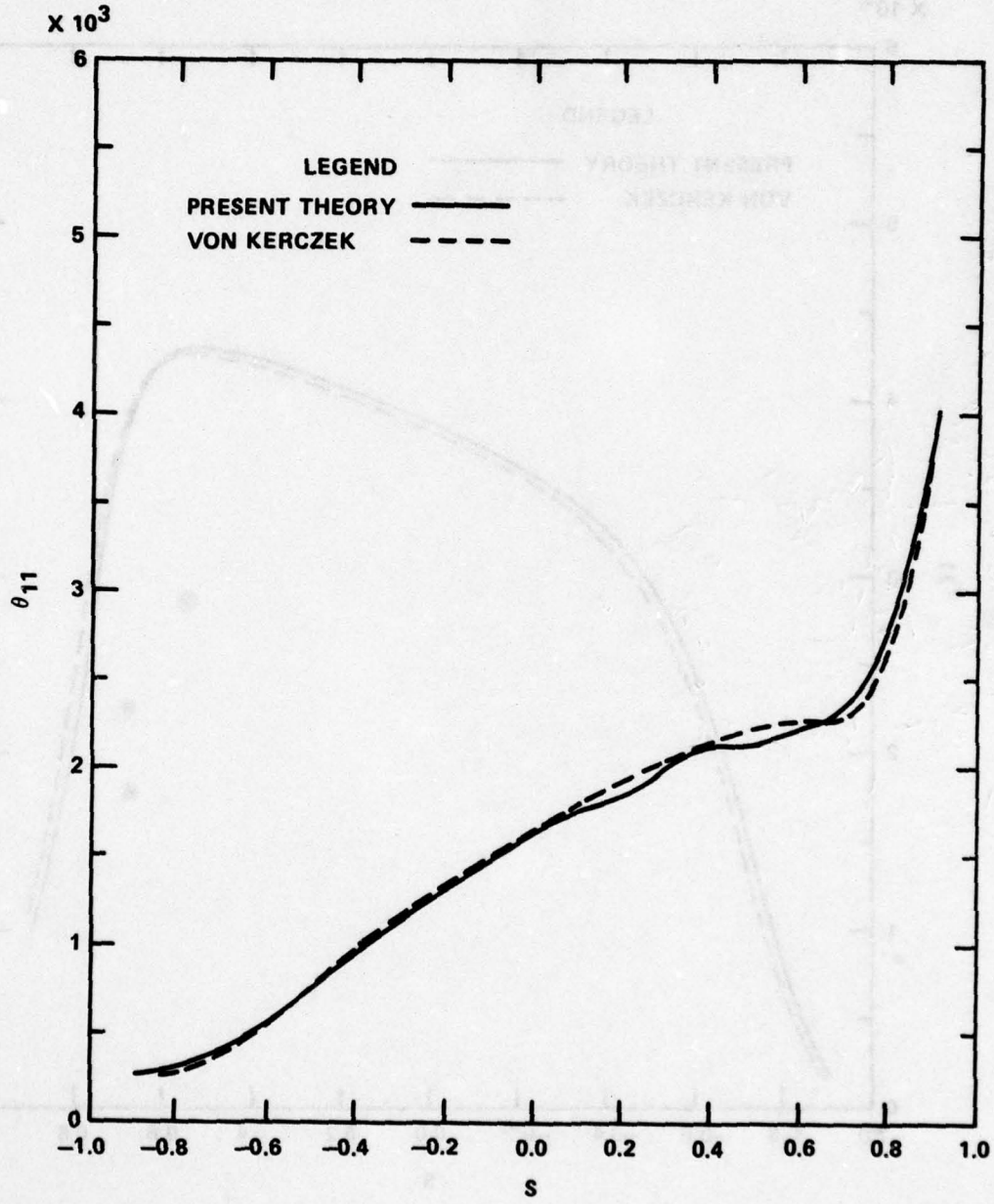

Figure 4c - Streamline 10

Figure 4 (Continued)

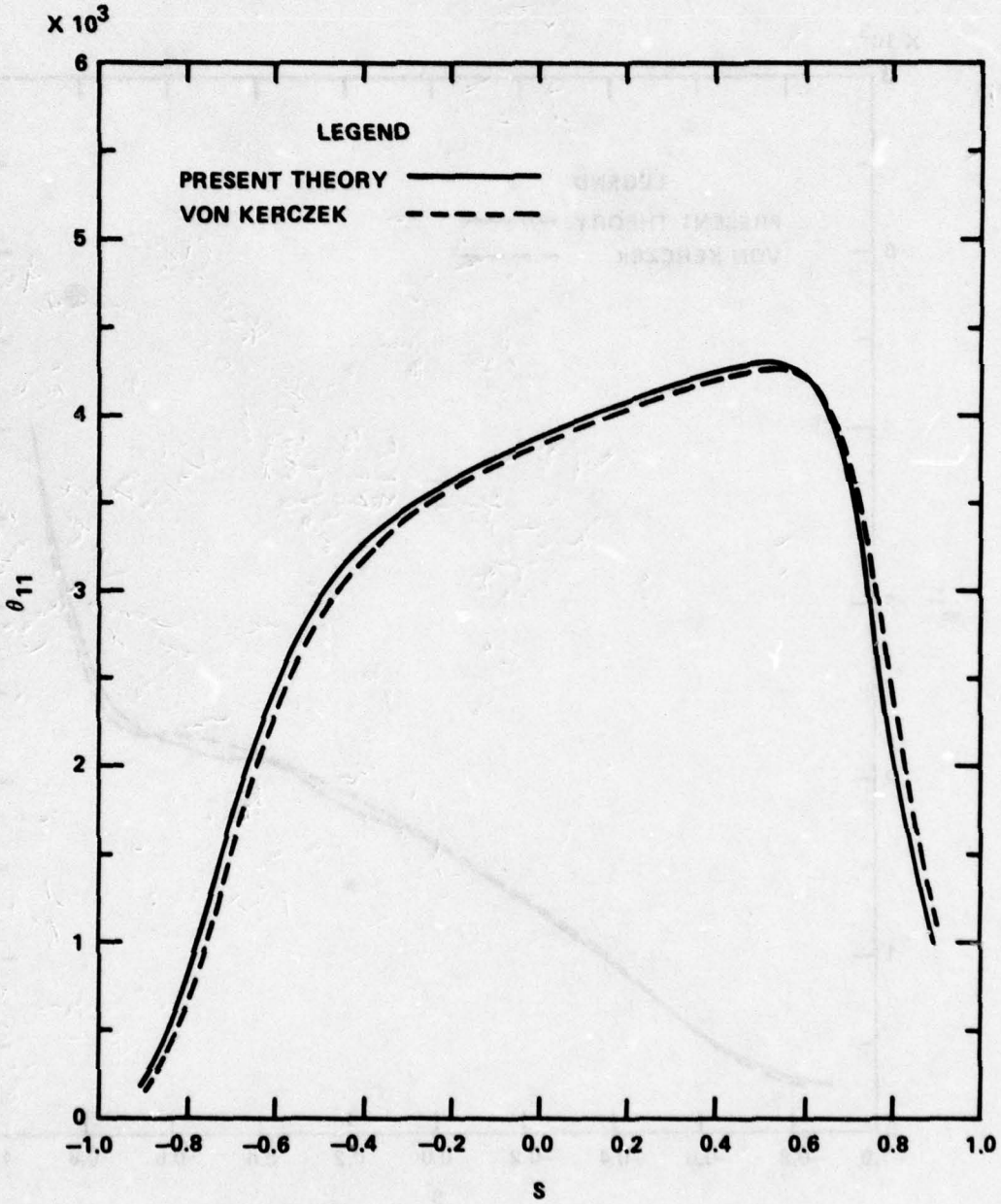

Figure 4d - Streamline 13

Figure 5 - Streamline Skin Friction Coefficient versus Axial Distance for Flow Along Streamlines of the Lucy Ashton

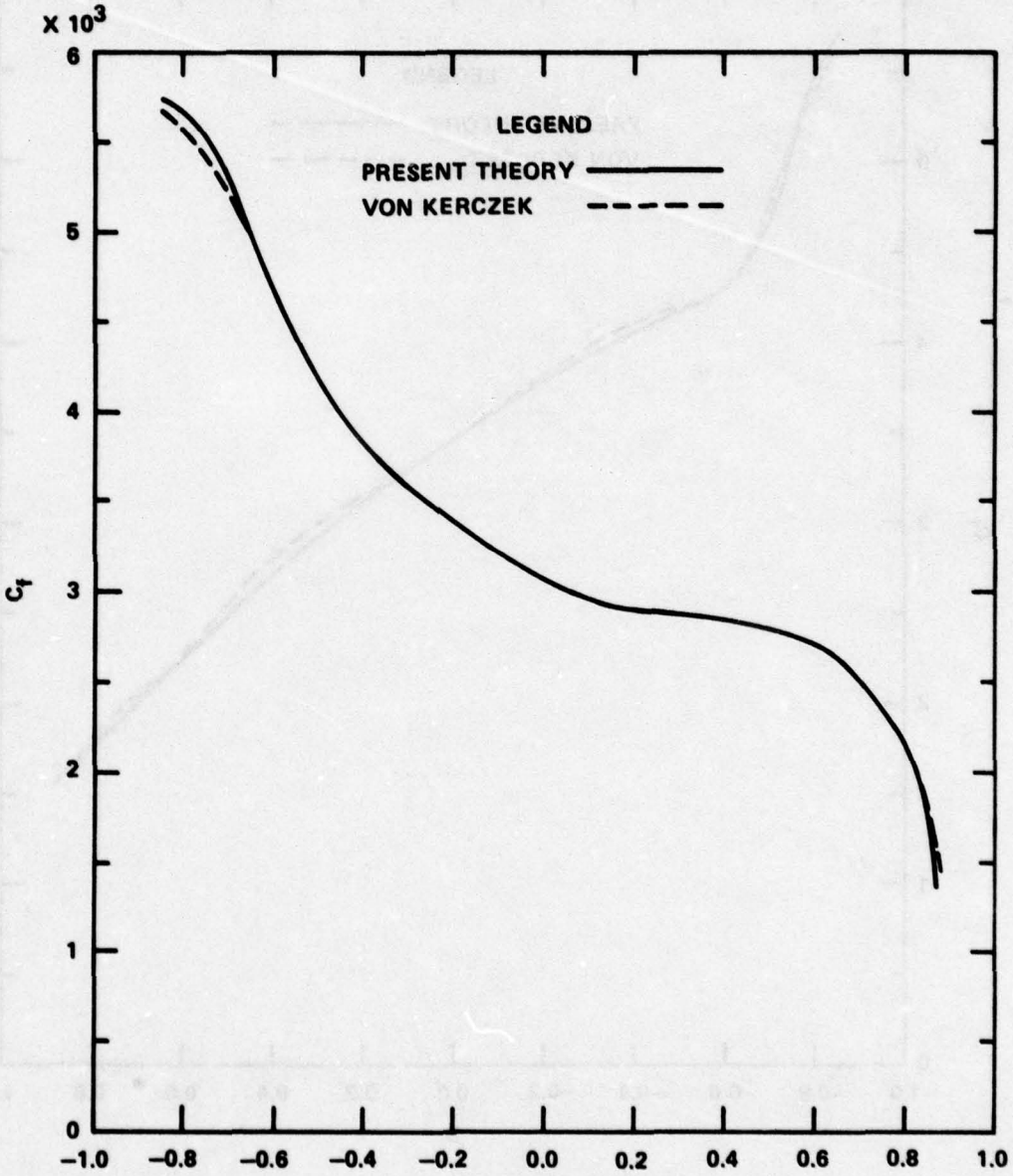

Figure 5a - Streamline 1

Figure 5 (Continued)

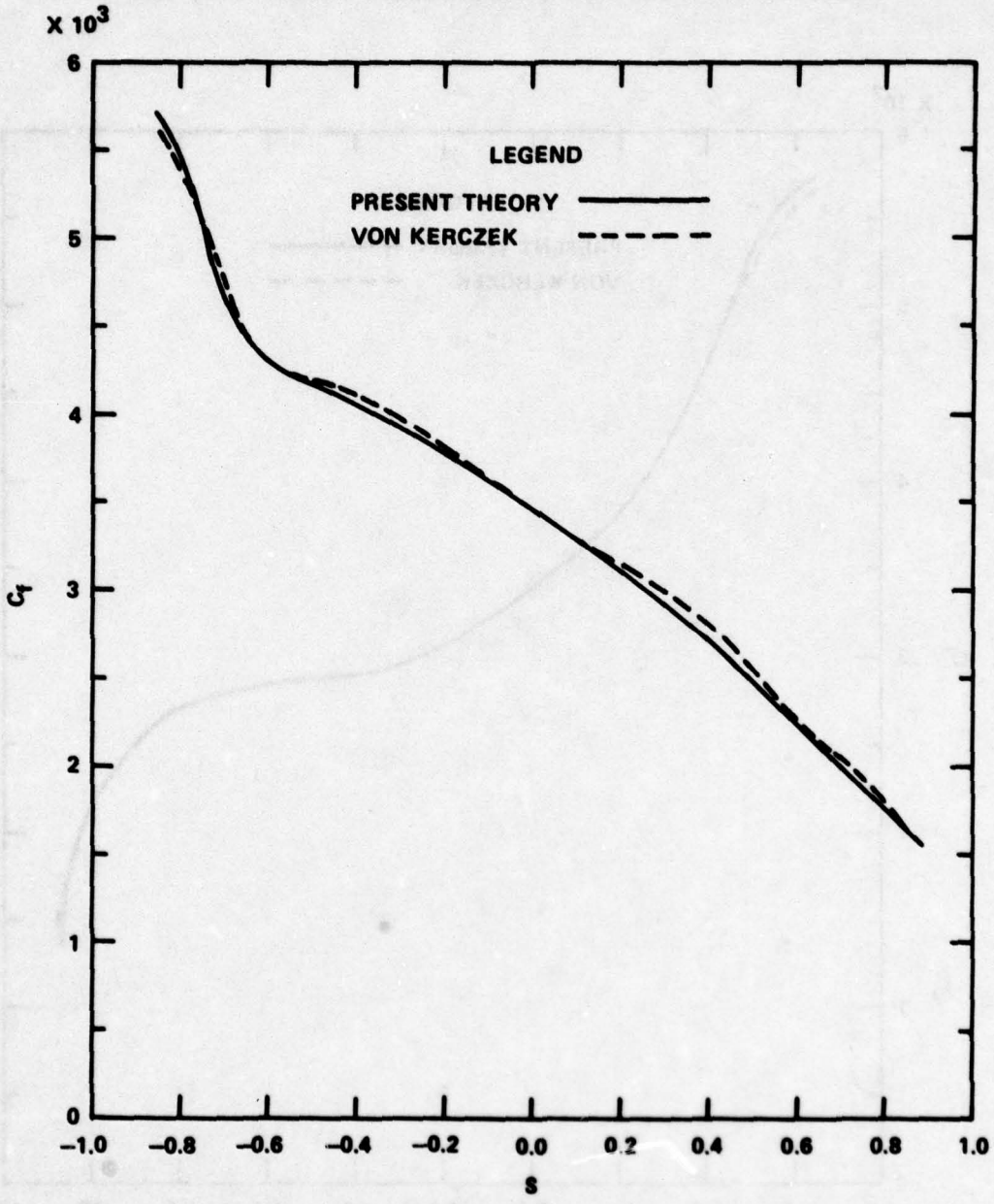

Figure 5b - Streamline 6

Figure 5 (Continued)

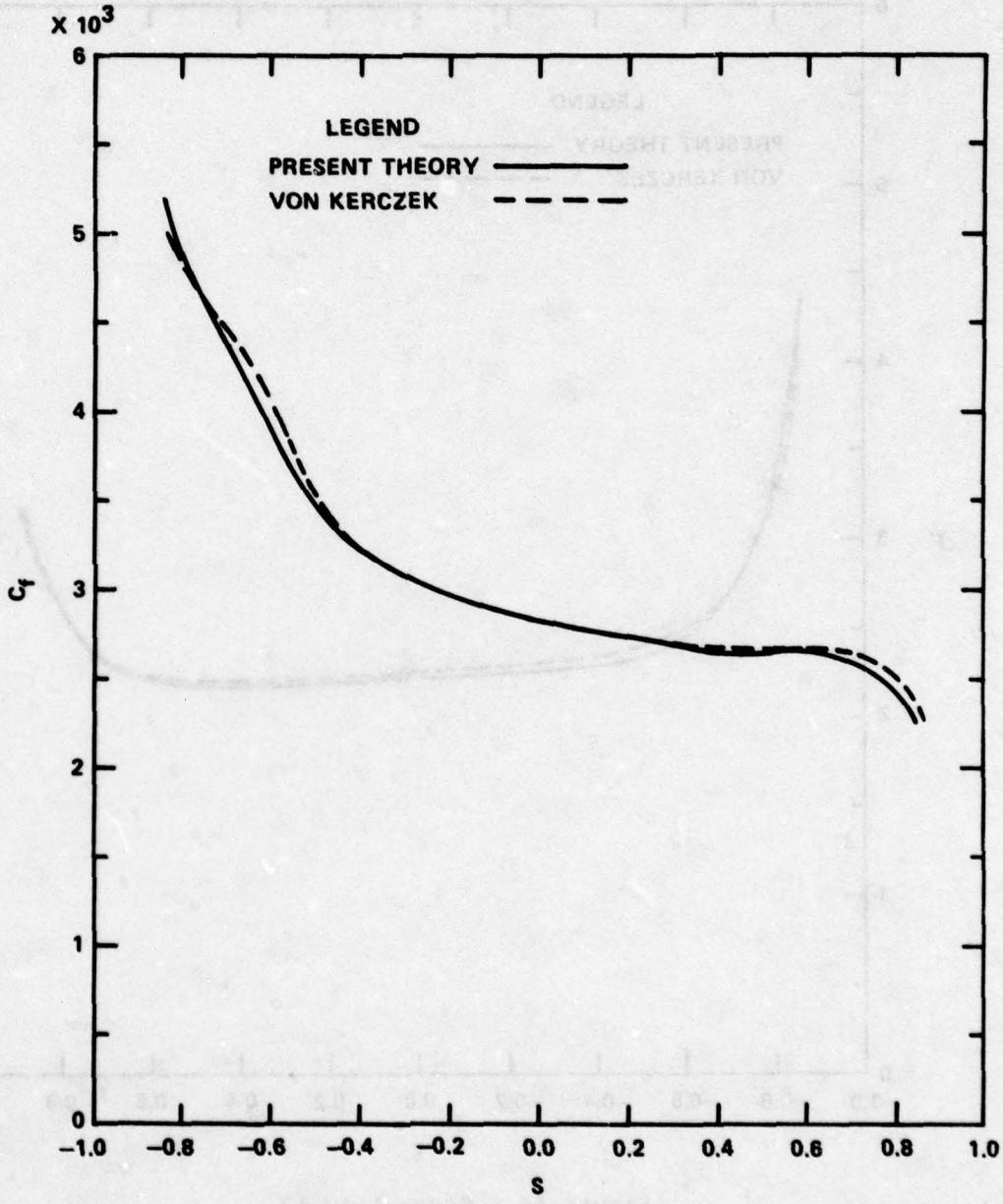

Figure 5c - Streamline 10

Figure 5 (Continued)

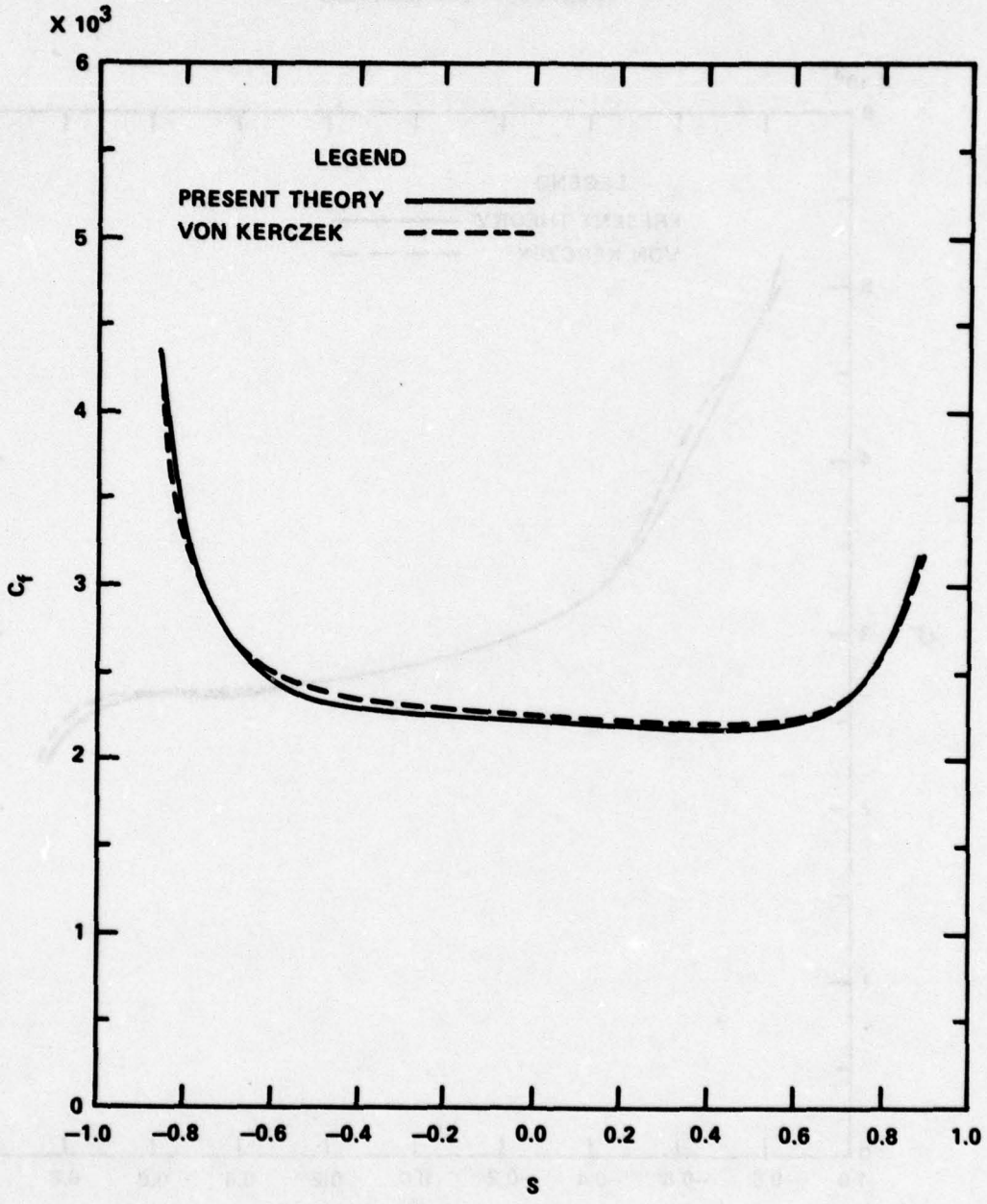

Figure 5d - Streamline 13

Figure 6 - Crossflow Angle versus Axial Distance for Flow Along Streamlines of the Lucy Ashton

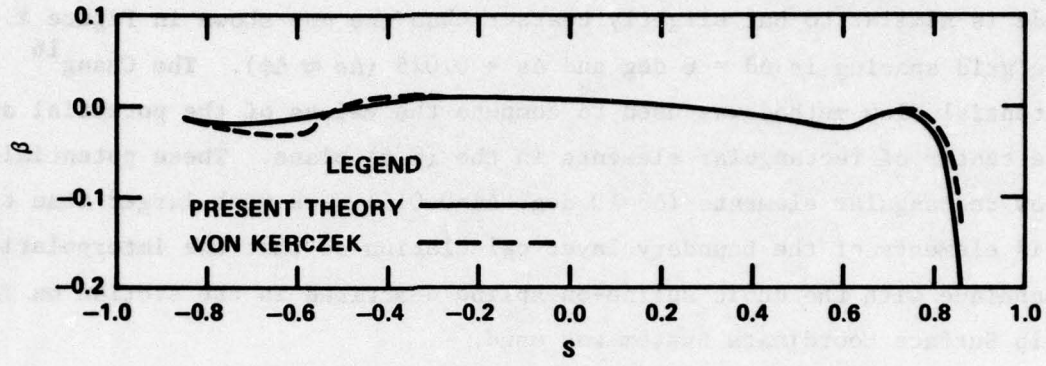

Figure 6a - Streamline 1

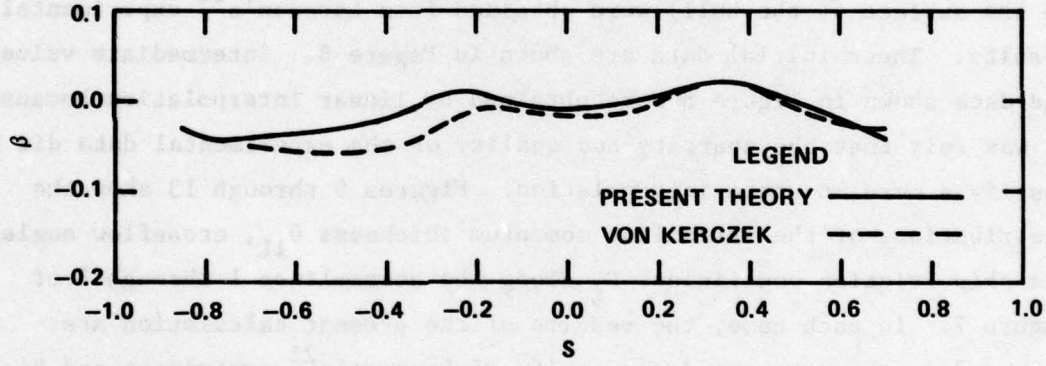

Figure 6b - Streamline 6

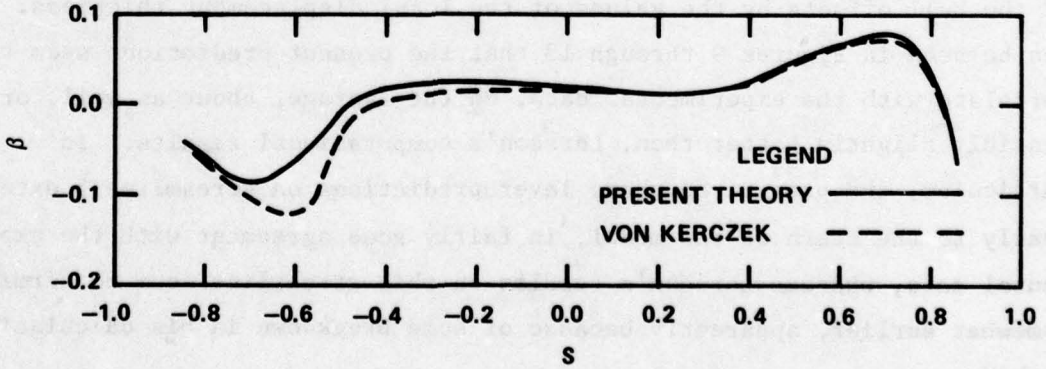

Figure 6c - Streamline 10

coordinate system and uses a numerical integration method that includes the crossflow terms by an explicit method. The present calculation scheme may improve on Larsson's results only in detail but not in a fundamental way.

The surface coordinate grid on which the present calculations were made is similar to but slightly coarser than the one shown in Figure 2. The grid spacing is $\Delta\theta$ = 6 deg and Δs = 0.025 ($\Delta s \approx \Delta\phi$). The Chang[16] potential flow method was used to compute the values of the potential at the center of rectangular elements in the (θ,ϕ) plane. These potential flow rectangular elements ($\Delta\theta$=10 deg, $\Delta\phi$=0.045) were much larger than the grid elements of the boundary layer calculation so that the interpolation technique with the cubic spline-on-spline described in the section on The Ship Surface Coordinate System was used.

Initial conditions for the quantities θ_{11}, H, and t = tan β at station s = -0.5 (which very nearly coincides with one of the θ-coordinate curves on the surface of the hull) were obtained from Larsson's[21] experimental results. These initial data are shown in Figure 8. Intermediate values of the data shown in Figure 8 were obtained by linear interpolation because it was felt that the sparsity and quality of the experimental data did not justify a more accurate interpolation. Figures 9 through 13 show the distributions of the streamline momentum thickness θ_{11}, crossflow angle β, and skin friction coefficient C_f along the streamlines 1 through 8 of Figure 7. In each case, the results of the present calculation are compared to the corresponding results of Larsson's[21] experiment and his calculation that includes the complete crossflow but not the modification of the hull offsets by the values of the local displacement thickness. It can be seen in Figures 9 through 13 that the present predictions seem to correlate with the experimental data, on the average, about as well, or possibly slightly better than, Larsson's computational results. In particular, the present boundary layer predictions on streamline 5 extend nearly to the stern of the model, in fairly good agreement with the experimental data, whereas Larsson's results on this streamline seem to terminate somewhat earlier, apparently because of some breakdown in his calculation method.

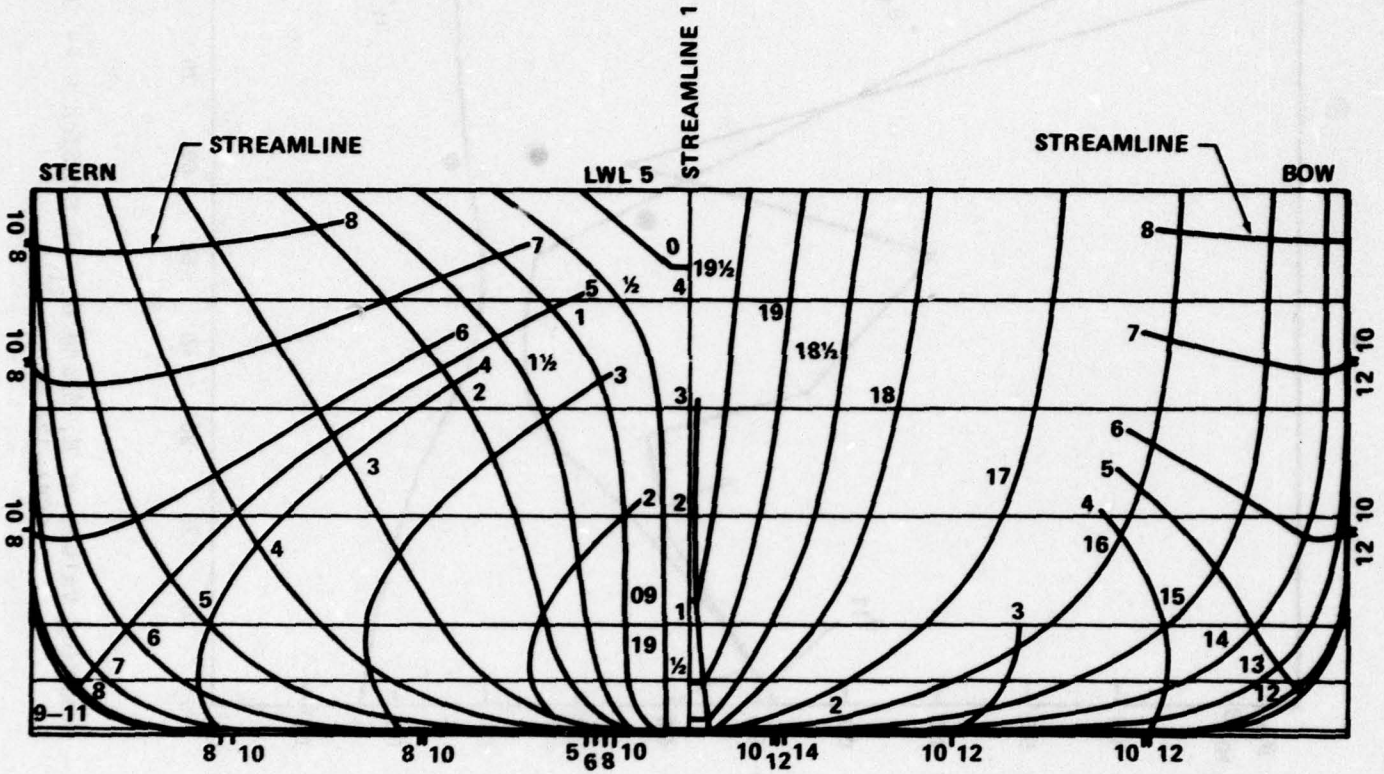

Figure 7 - Streamlines on the SSPA-720 Model Along Which Larsson Measured the Boundary Layer

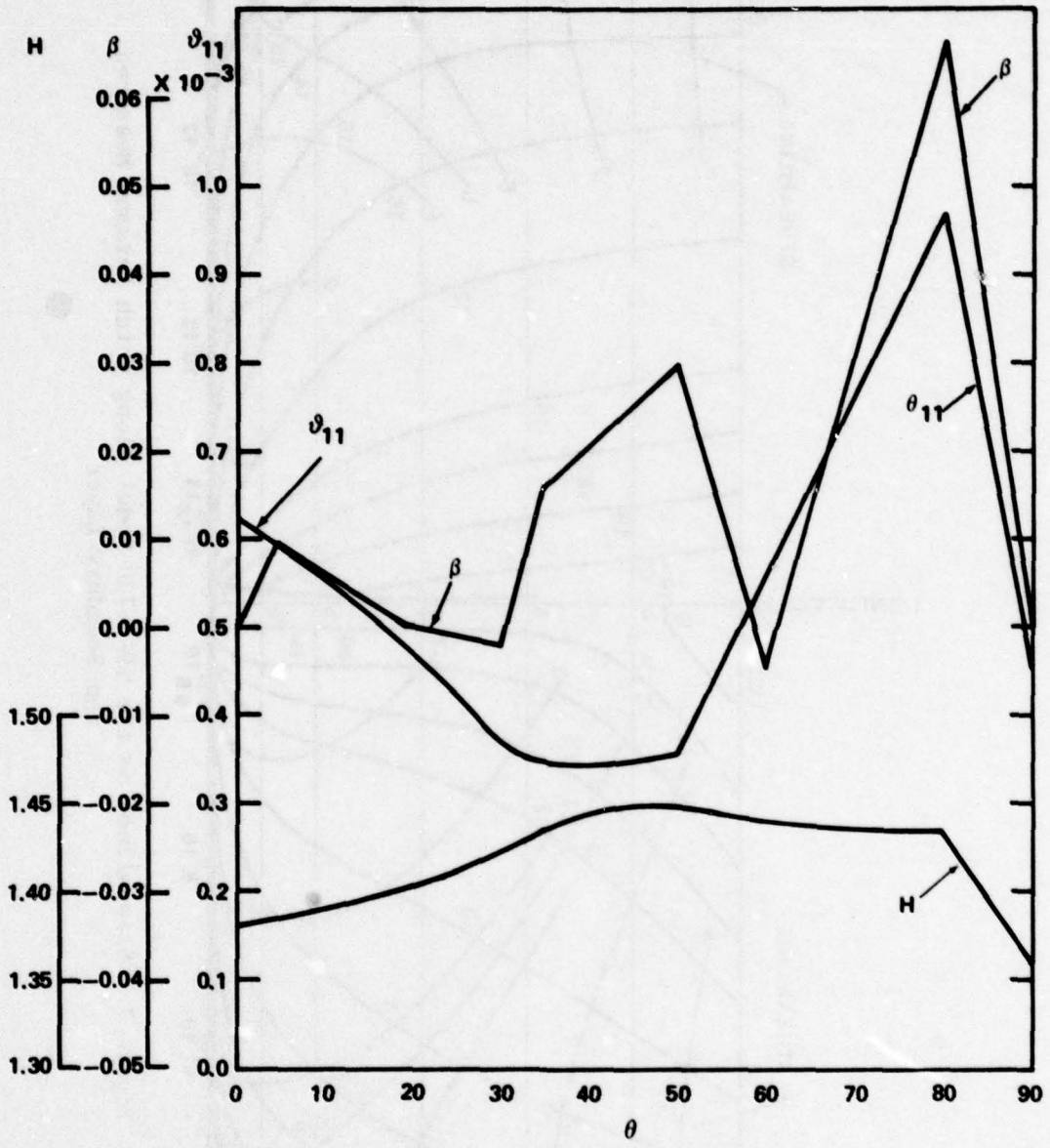

Figure 8 - Starting Values of H, β and θ_{11} at Station S =- 0.5 on SSPA-720 Model

Figure 9 - Boundary Layer Characteristics versus Axial Distance for Flow Along Streamline 1 on Model SSPA-720

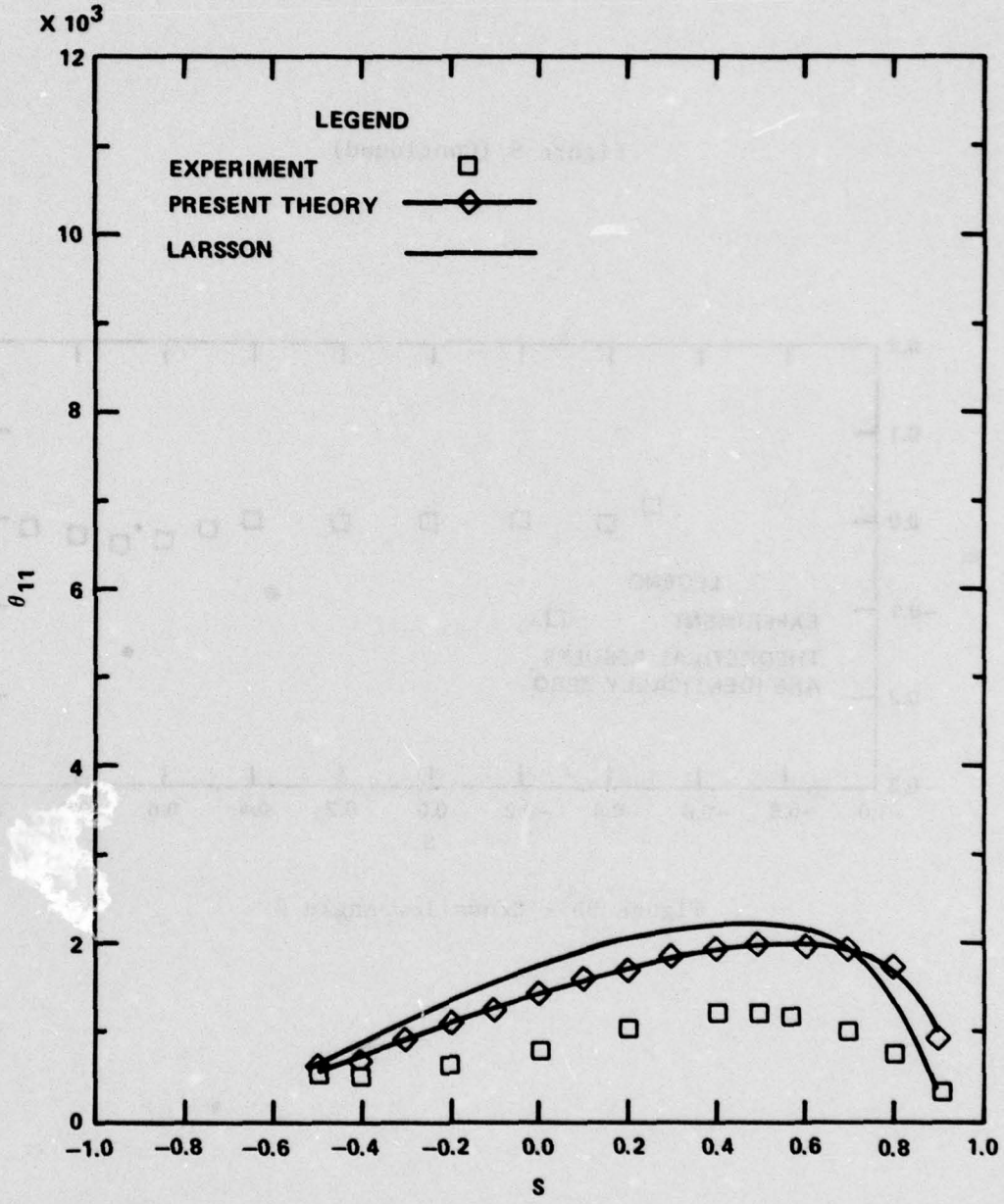

Figure 9a - Streamline Momentum Thickness

Figure 9 (Continued)

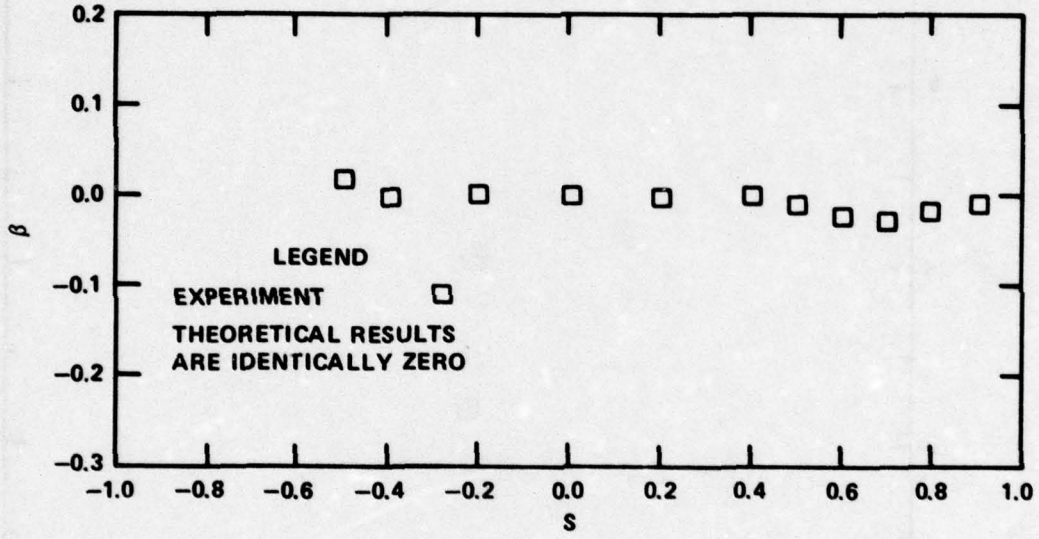

Figure 9b - Crossflow Angle β

Figure 9 (Continued)

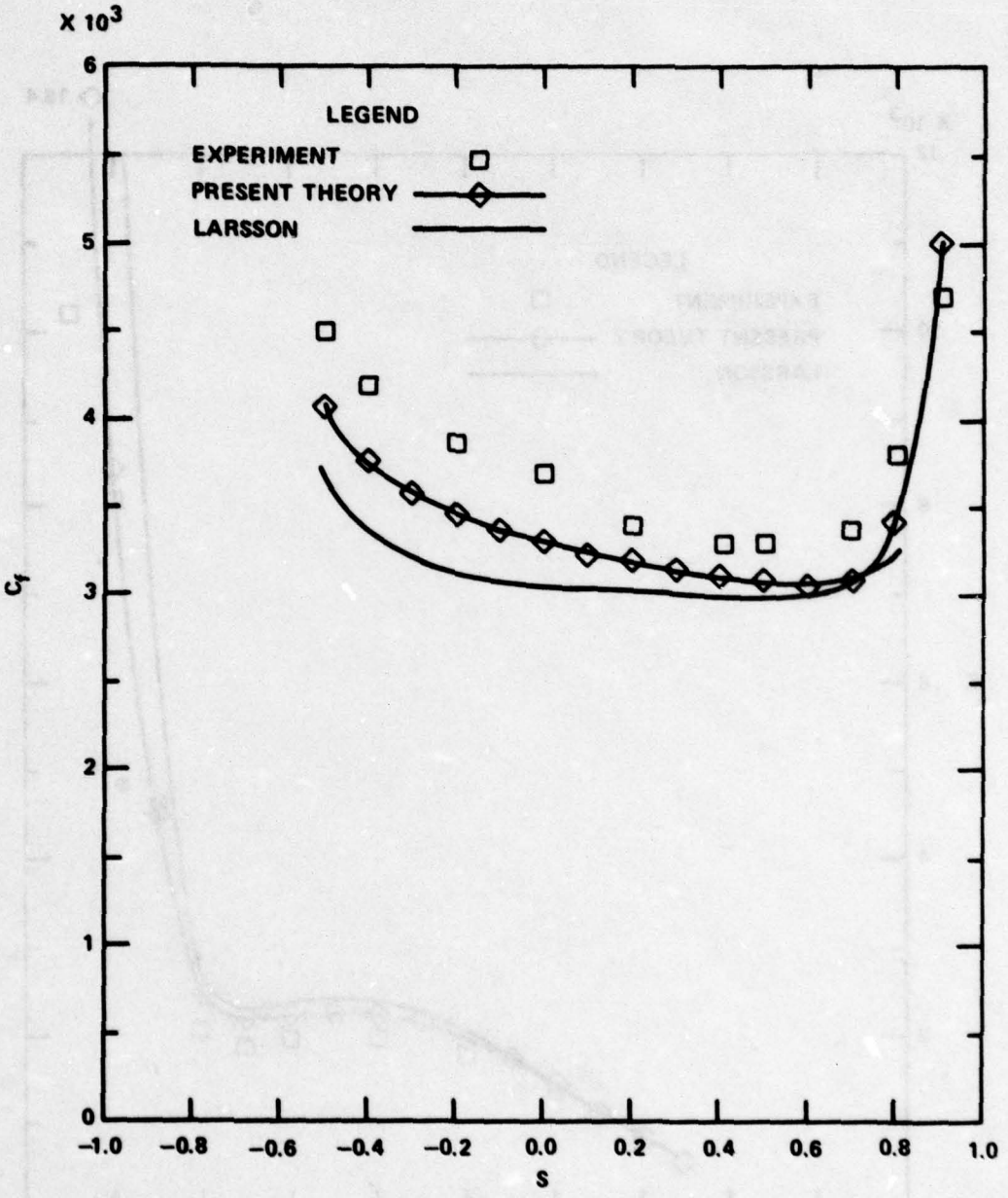

Figure 9c - Streamline Skin Friction Coefficient

Figure 10 - Boundary Layer Characteristics versus Axial Distance for Flow Along Streamline 3 on Model SSPA-720

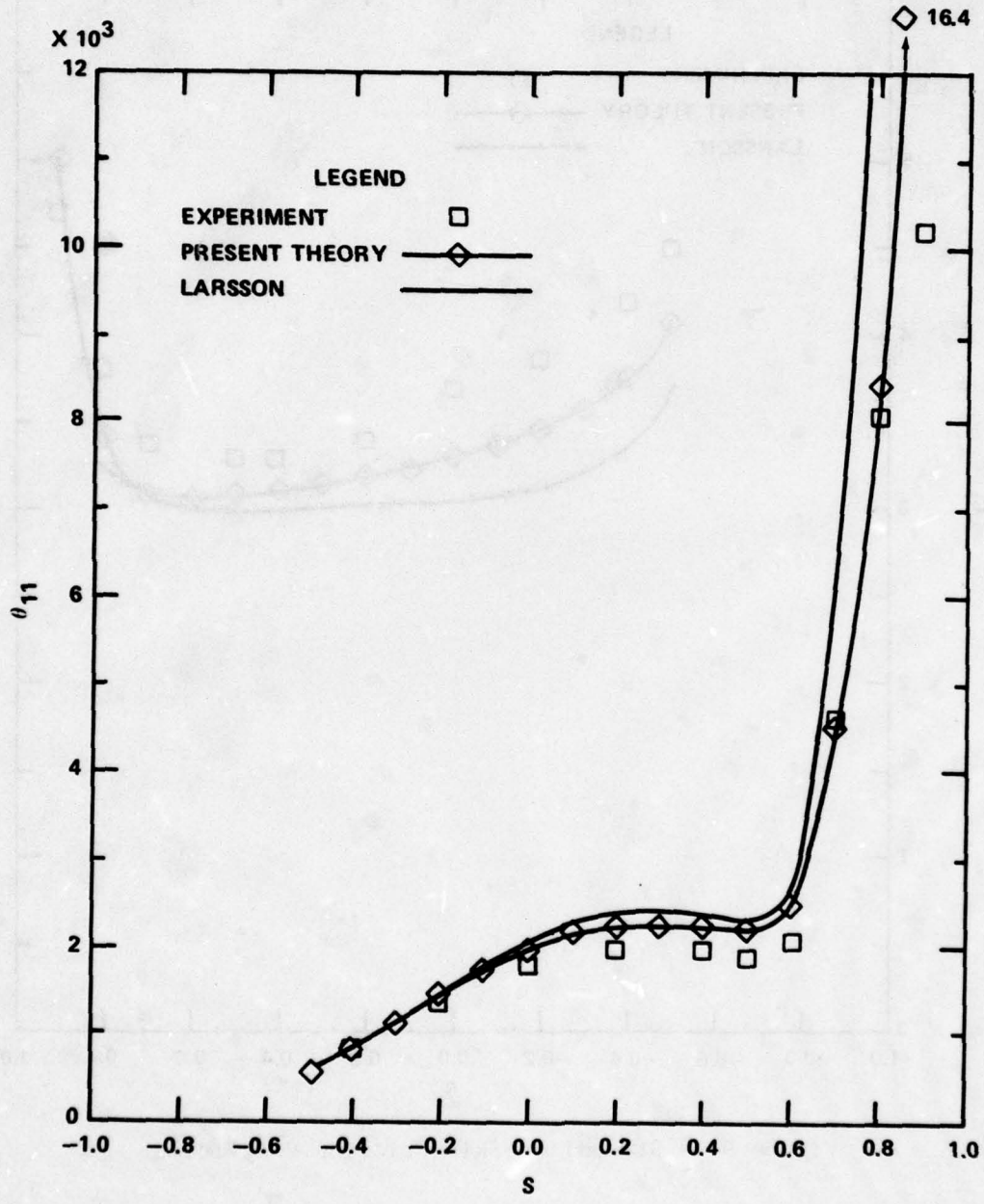

Figure 10a - Streamline Momentum Thickness

Figure 10 (Continued)

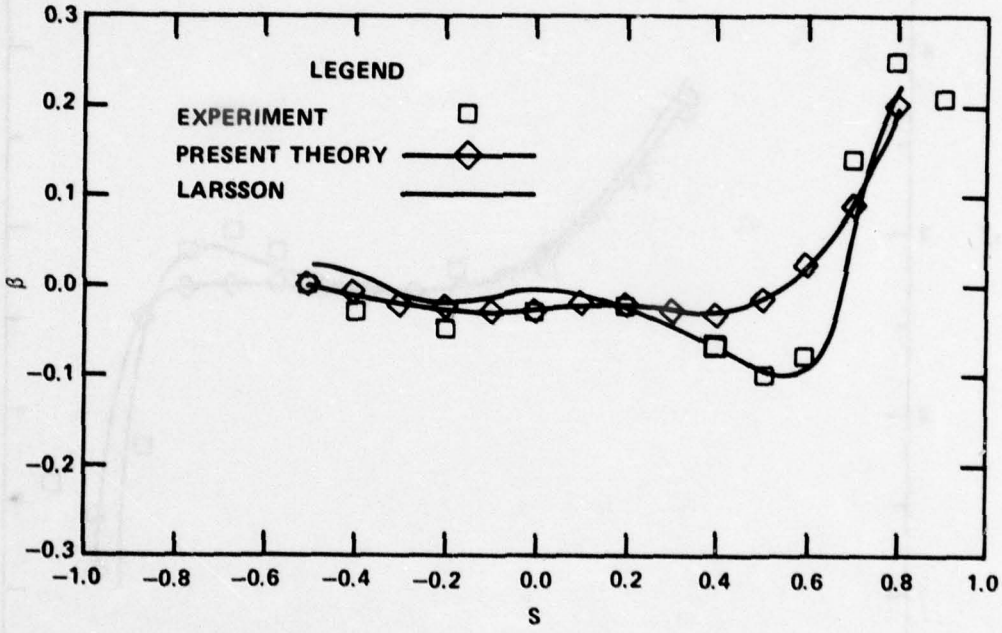

Figure 10b - Crossflow Angle β

Figure 10 (Continued)

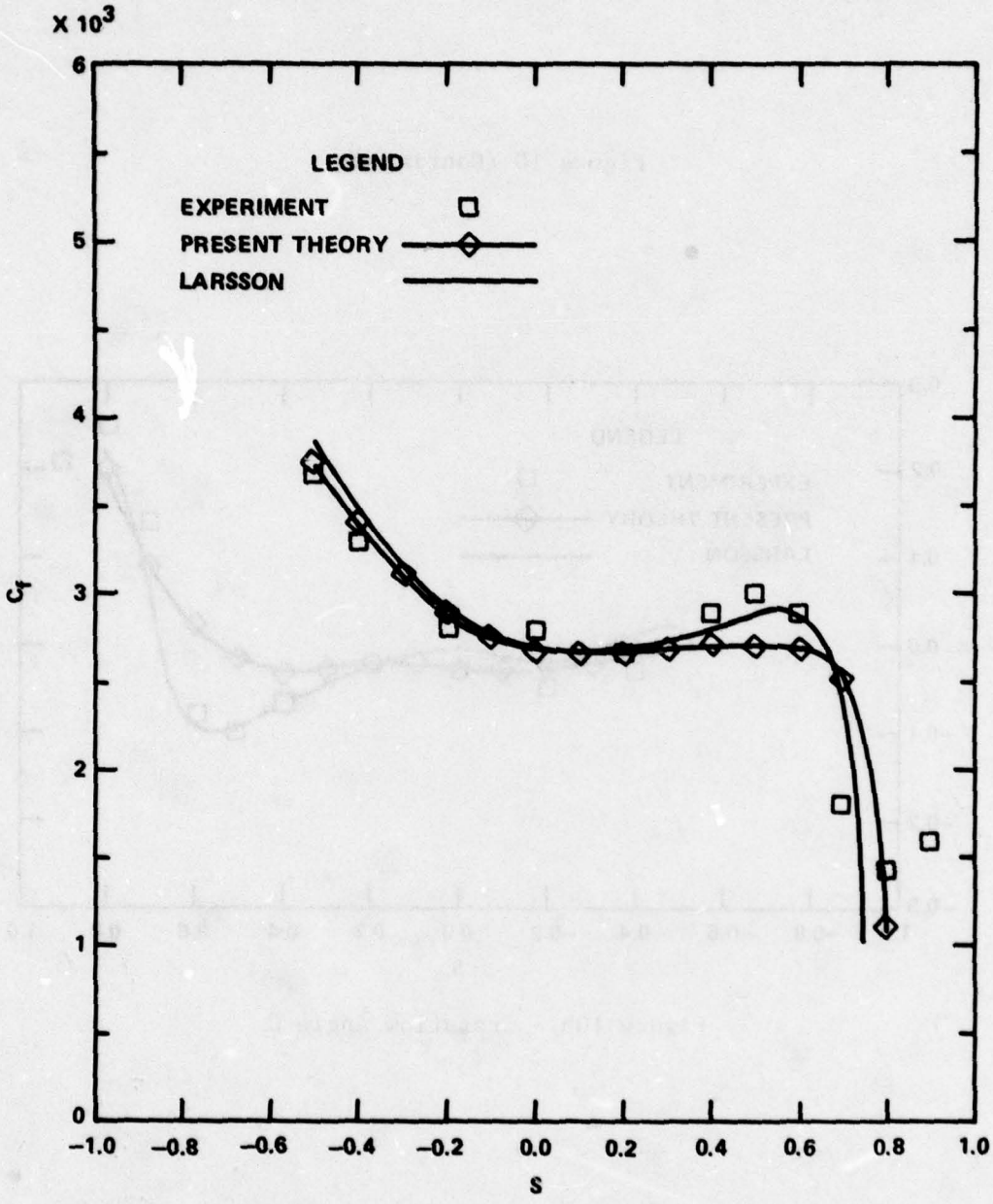

Figure 10c - Streamline Skin Friction Coefficient

Figure 11 - Boundary Layer Characteristics versus Axial Distance for Flow Along Streamline 5 on Model SSPA-720

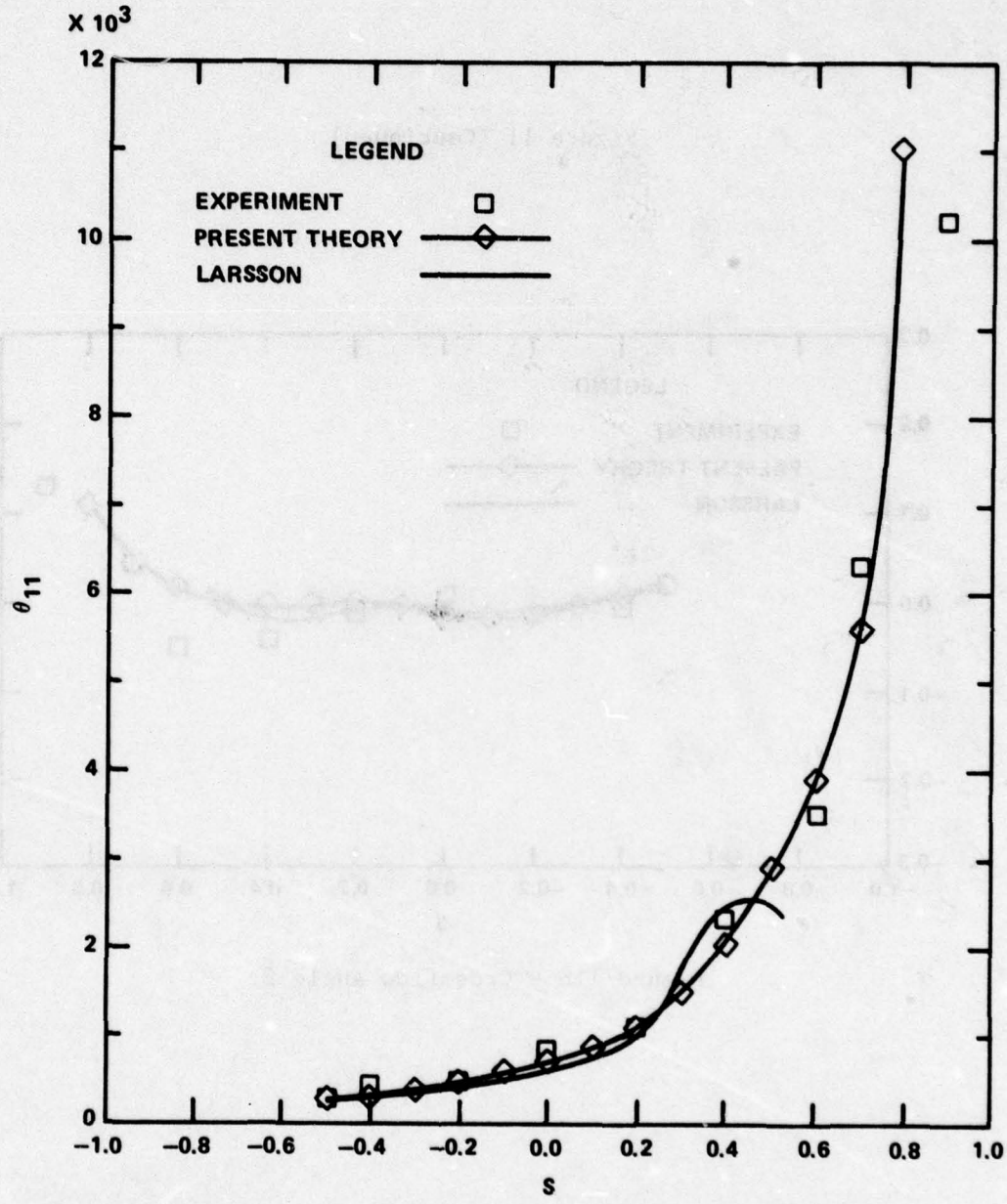

Figure 11a - Streamline Momentum Thickness

Figure 11 (Continued)

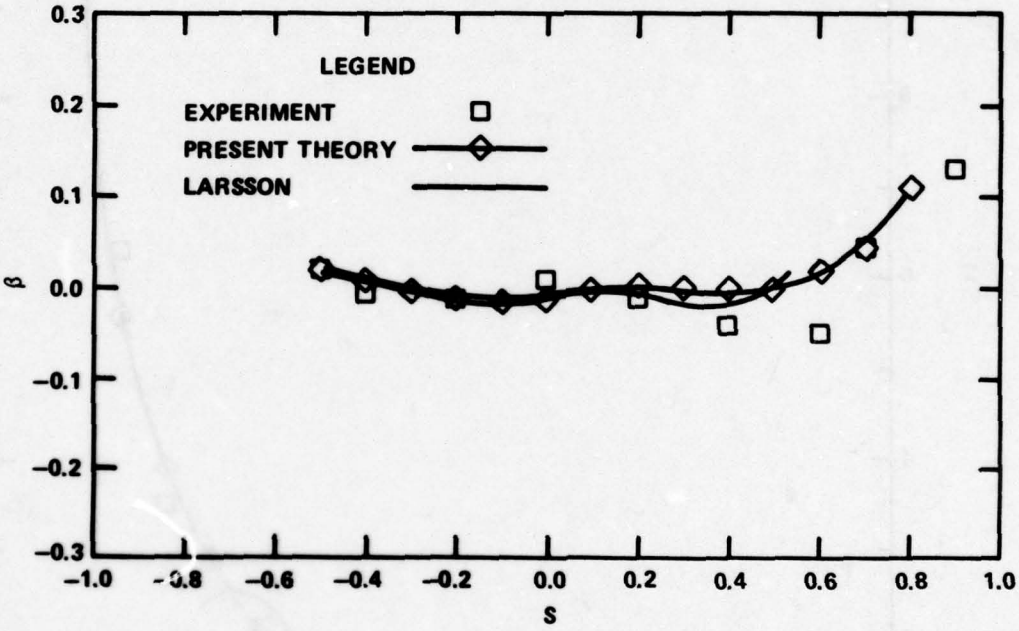

Figure 11b - Crossflow Angle β

Figure 11 (Continued)

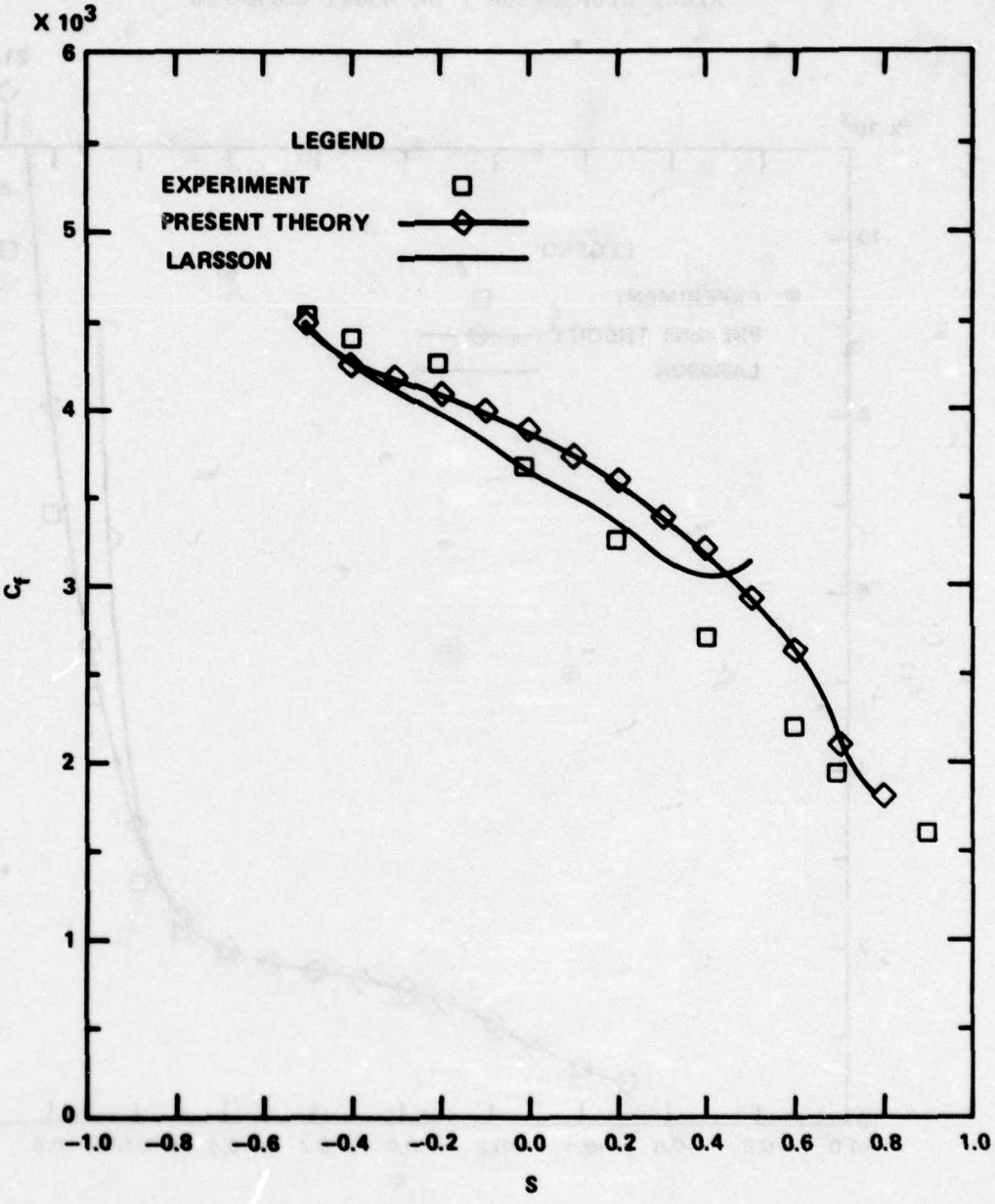

Figure 11c - Streamline Skin Friction Coefficient

Figure 12 - Boundary Layer Characteristics versus Axial Distance for Flow Along Streamline 7 on Model SSPA-720

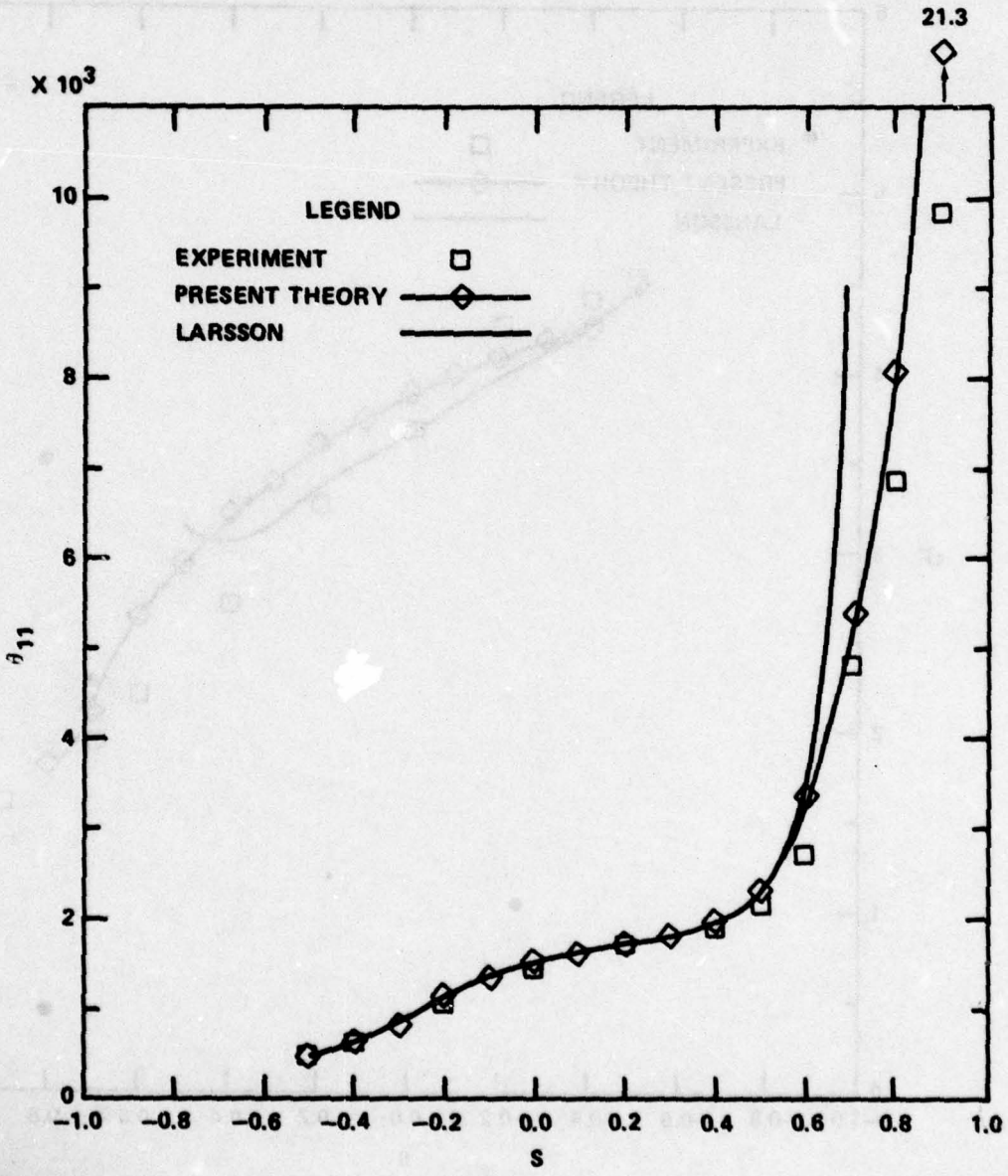

Figure 12a - Streamline Momentum Thickness

Figure 12 (Continued)

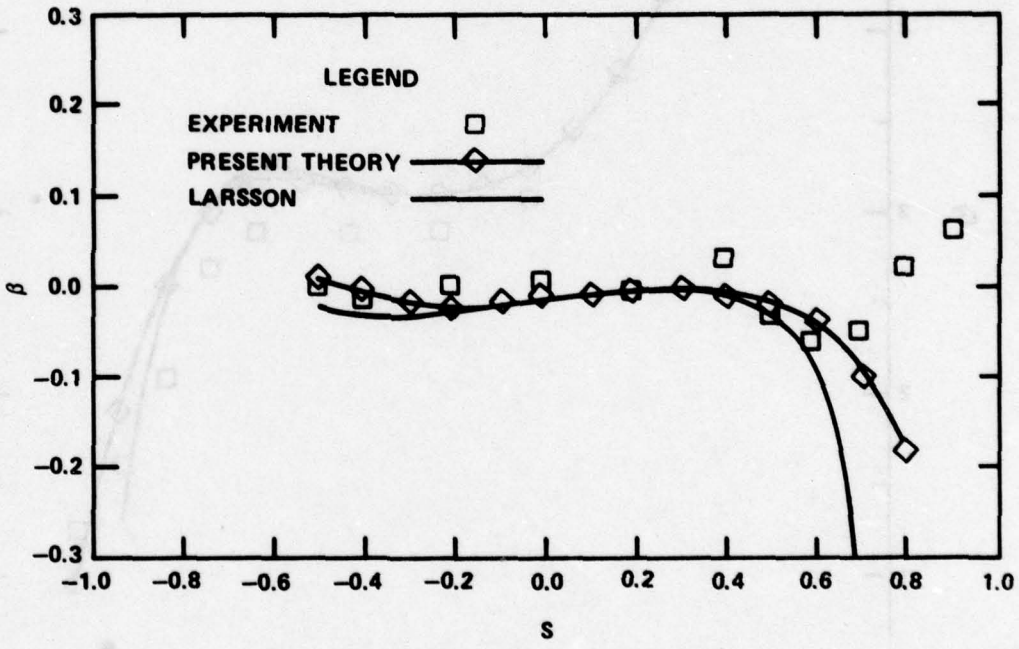

Figure 12b - Crossflow Angle β

Figure 12 (Continued)

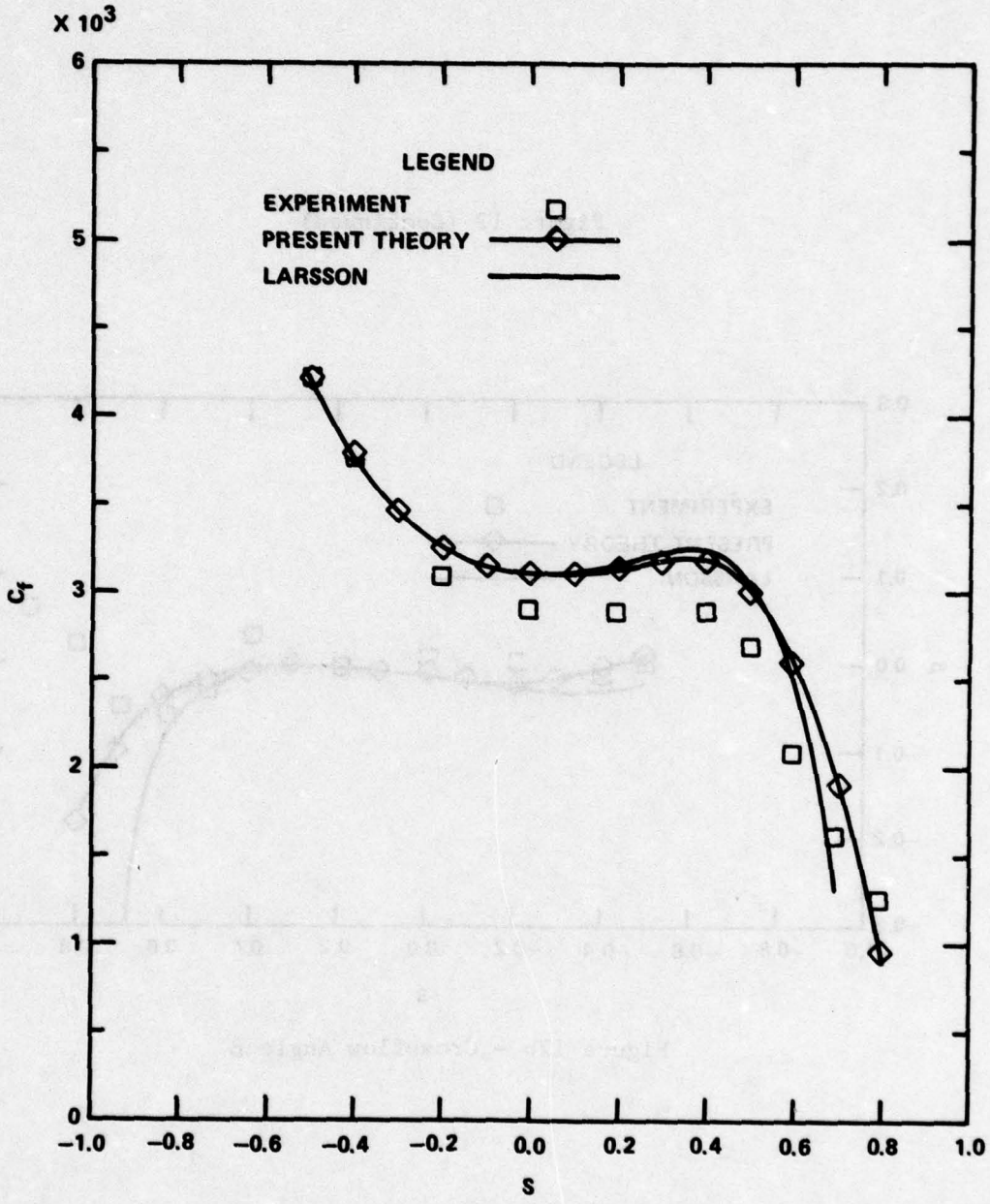

Figure 12c - Streamline Skin Friction Coefficient

Figure 13 - Boundary Layer Characteristics versus Axial Distance for Flow Along Streamline 8 on Model SSPA-720

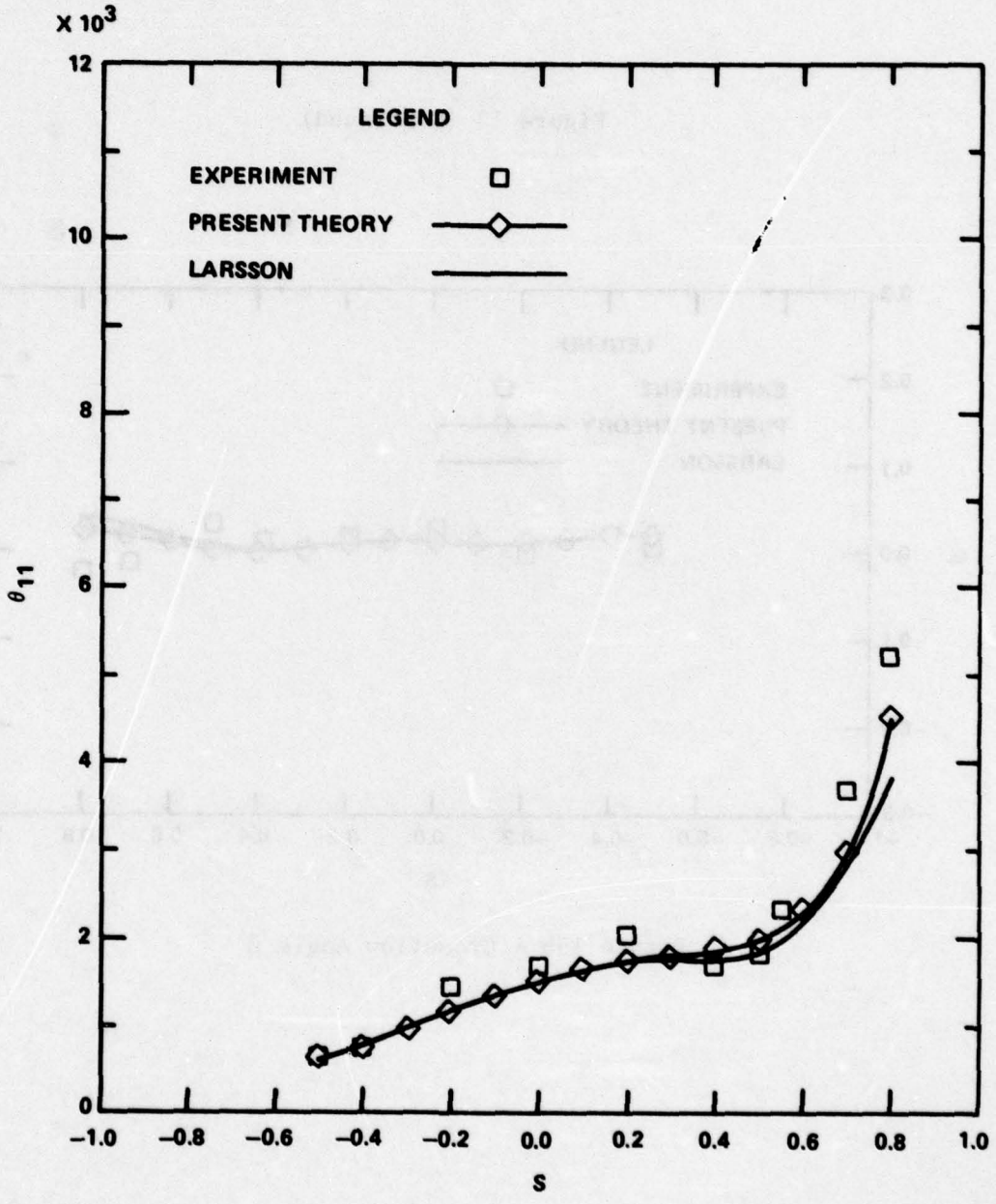

Figure 13a - Streamline Momentum Thickness

Figure 13 (Continued)

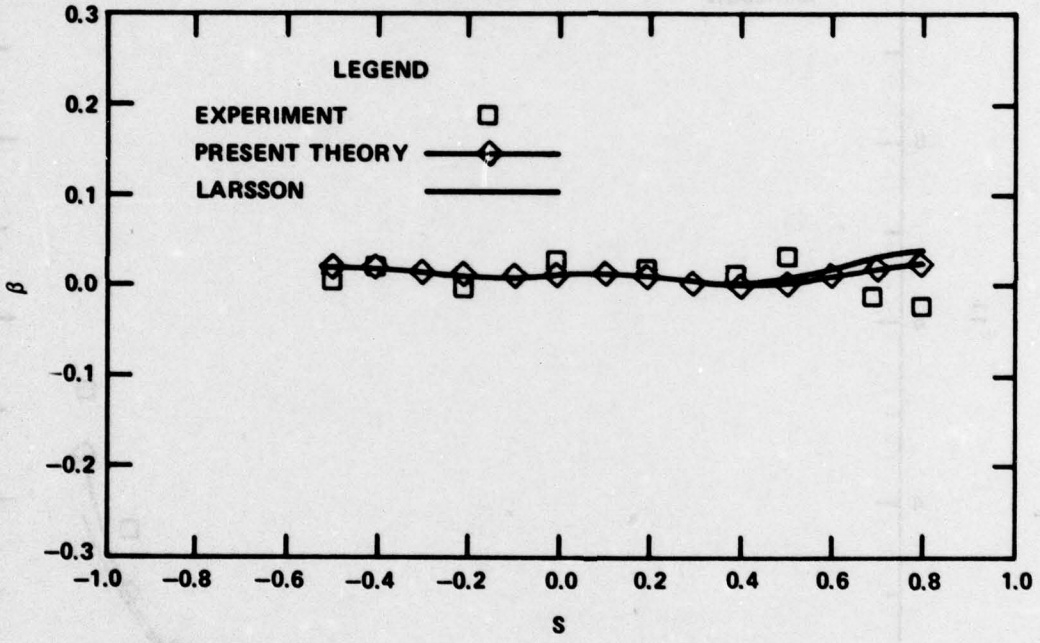

Figure 13b - Crossflow Angle β

Figure 13 (Continued)

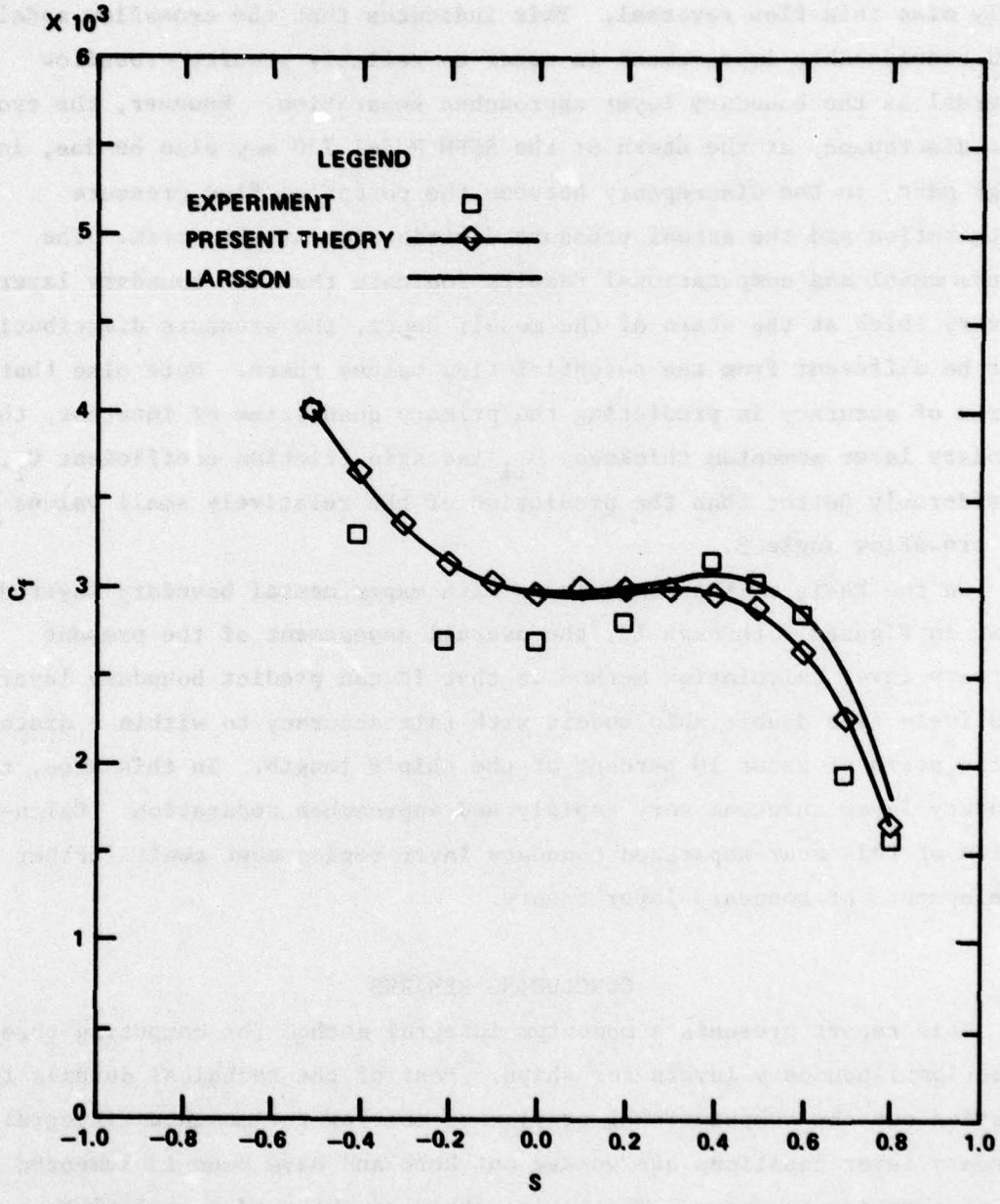

Figure 13c - Streamline Skin Friction Coefficient

It is to be noted that the experimental values of the crossflow angle β shown in Figures 9b, 10b, 11b, 12b, and 13b all exhibit a change in sign (hence crossflow reversal) between the stations $s = 0.6$ and $s = 0.8$. The results of the boundary layer calculations shown in these figures consistently miss this flow reversal. This indicates that the crossflow model may need considerable improvement in order to reliably predict crossflow reversal as the boundary layer approaches separation. However, the crossflow discrepancy at the stern of the SSPM Model 720 may also be due, in large part, to the discrepancy between the potential flow pressure distribution and the actual pressure distribution at the stern. The experimental and computational results indicate that the boundary layer is very thick at the stern of the model; hence, the pressure distribution must be different from the potential flow values there. Note also that the degree of accuracy in predicting the primary quantities of interest, the boundary layer momentum thickness θ_{11} and skin friction coefficient C_f, is considerably better than the prediction of the relatively small values of the crossflow angle β.

On the basis of the comparisons with experimental boundary layer data shown in Figures 9 through 13, the overall assessment of the present boundary layer calculation method is that it can predict boundary layers on relatively fine double ship models with fair accuracy to within a distance of the stern of about 10 percent of the ship's length. In this area, the boundary layer thickens very rapidly and approaches separation. Calculation of this near-separated boundary layer region must await further developments of boundary layer theory.

CONCLUDING REMARKS

This report presents a momentum integral method for computing three-dimensional boundary layers for ships. Most of the technical details for carrying out the computational problem of solving the momentum-integral boundary layer equations are worked out here and have been implemented in a set of computer programs. The basic method can be used to calculate

certain boundary layer parameters, such as boundary layer thickness or skin friction, with fair accuracy over a large portion of hulls where unseparated flow is maintained. The computer programs are now ready to be modified so as to improve the crossflow modeling, with whatever new experimental data becomes available. Alternatively, portions of the developments described in this report, such as the surface coordinate system and inviscid flow calculation, can be used in other methods for calculating the boundary layer.

APPENDIX
MATHEMATICAL DETAILS

Substituting directly from Equation (21) into Equation (6) yields

$$\Theta_{11} = \theta_{11}\,[\cos^2\alpha - t(\bar{f}_1+\bar{f}_2)\,\sin\alpha\cos\alpha + t^2\bar{f}_3\,\sin^2\alpha] \equiv \theta_{11}g_{11}(t,H) \qquad (49a)$$

$$\Theta_{12} = \theta_{11}\,[(1-t^2\bar{f}_3)\,\sin\alpha\cos\alpha + t\bar{f}_2\,\cos^2\alpha - t\bar{f}_1\,\sin^2\alpha] \equiv \theta_{11}g_{12}(t,H) \qquad (49b)$$

$$\Theta_{21} = \theta_{11}\,[(1-t^2\bar{f}_3)\,\sin\alpha\cos\alpha + t\bar{f}_1\,\cos^2\alpha - t\bar{f}_2\,\sin^2\alpha] \equiv \theta_{11}g_{21}(t,H) \qquad (49c)$$

$$\Theta_{22} = \theta_{11}\,[\sin^2\alpha + t(\bar{f}_1+\bar{f}_2)\,\sin\alpha\cos\alpha + t^2\bar{f}_3\,\cos^2\alpha] \equiv \theta_{11}g_{22}(t,H) \qquad (49d)$$

$$\Delta_1 = \theta_{11}\,(H\cos\alpha - t\bar{f}_4\,\sin\alpha) \equiv \theta_{11}h_1(t,H) \qquad (49e)$$

$$\Delta_2 = \theta_{11}\,(H\sin\alpha + t\bar{f}_4\,\cos\alpha) \equiv \theta_{11}h_2(t,H) \qquad (49f)$$

The momentum integral Equations (3) can then be written

$$g_{11}\frac{\partial\theta_{11}}{\partial\ell_\phi} + \theta_{11}\frac{\partial g_{11}}{\partial t}\frac{\partial t}{\partial\ell_\phi} + \theta_{11}\frac{\partial g_{11}}{\partial H}\frac{\partial H}{\partial\ell_\phi} + g_{12}\frac{\partial\theta_{11}}{\partial\ell_\theta}$$

$$+ \theta_{11}\frac{\partial g_{12}}{\partial t}\frac{\partial t}{\partial\ell_\theta} + \theta_{11}\frac{\partial g_{12}}{\partial H}\frac{\partial H}{\partial\ell_\theta} = C_1(\theta_{11},t,H) \qquad (50a)$$

and

$$g_{21}\frac{\partial\theta_{11}}{\partial\ell_\phi} + \theta_{11}\frac{\partial g_{21}}{\partial t}\frac{\partial t}{\partial\ell_\phi} + \theta_{11}\frac{\partial g_{21}}{\partial H}\frac{\partial H}{\partial\ell_\phi} + g_{22}\frac{\partial\theta_{11}}{\partial\ell_\theta}$$

$$+ \theta_{11}\frac{\partial g_{22}}{\partial t}\frac{\partial t}{\partial\ell_\theta} + \theta_{11}\frac{\partial g_{22}}{\partial H}\frac{\partial H}{\partial\ell_\theta} = C_2(\theta_{11},t,H) \qquad (50b)$$

where

$$C_1 = \frac{1}{2} C_{f_\phi} - \Theta_{11} \frac{2}{U} \frac{\partial U}{\partial \ell_\phi} - 2 \frac{\Theta_{12}}{U} \frac{\partial U}{\partial \ell_\theta} - \frac{1}{U} \left(\Delta_1 \frac{\partial u_\phi}{\partial \ell_\phi} + \Delta_2 \frac{\partial u_\phi}{\partial \ell_\theta} \right)$$

$$+ K_\phi \left(\Theta_{11} - \Theta_{22} - \frac{\Delta_2 u_\theta}{U} \right) + K_\theta \left(\Theta_{12} + \Theta_{21} + \frac{\Delta_1 u_\theta}{U} \right)$$

Use is made here of the identity

$$\Theta_{12} = \Theta_{21} - \Delta_2 \frac{u_\phi}{U} + \Delta_1 \frac{u_\theta}{U}$$

Hence,

$$C_1(\theta_{11}, t, H) = \frac{1}{2} C_{f_\phi} - \frac{2\theta_{11}}{U} \left(g_{11} \frac{\partial U}{\partial \ell_\phi} + g_{12} \frac{\partial U}{\partial \ell_\theta} \right) - \frac{1}{U} \left(\Delta_1 \frac{\partial u_\phi}{\partial \ell_\phi} + \Delta_2 \frac{\partial u_\phi}{\partial \ell_\theta} \right)$$

$$+ K_\phi \theta_{11} (g_{11} - g_{22} - h_2 \sin \alpha) + K_\theta \theta_{11} (g_{12} + g_{21} + h_1 \sin \alpha) \quad (51a)$$

Similarly,

$$C_2(\theta_{11}, t, H) = \frac{1}{2} C_{f_\phi} - \frac{2\theta_{11}}{U} \left(g_{21} \frac{\partial U}{\partial \ell_\phi} + g_{22} \frac{\partial U}{\partial \ell_\theta} \right) - \frac{1}{U} \left(\Delta_1 \frac{\partial u_\theta}{\partial \ell_\phi} + \Delta_2 \frac{\partial u_\theta}{\partial \ell_\theta} \right)$$

$$+ K_\theta \theta_{11} (g_{22} - g_{11} - h_1 \cos \alpha) + K_\phi \theta_{11} (g_{21} + g_{12} + h_2 \cos \alpha) \quad (51b)$$

Let T and S be defined by

$$T = \frac{1}{U} (u_\phi \delta - U\Delta_1) \quad (52a)$$

and

$$S = \frac{1}{U} (u_\theta \delta - U\Delta_2) \quad (52b)$$

The entrainment Equation (7) can then be written in the form:

$$\frac{\partial T}{\partial \ell_\phi} + \frac{\partial S}{\partial \ell_\theta} = F(H) - \frac{T}{U_s}\frac{\partial U_s}{\partial \ell_\phi} - \frac{S}{U_s}\frac{\partial U_s}{\partial \ell_\theta} + TK_\phi + SK_\theta \tag{53}$$

Moreover, using Equations (10), (49e), and (49f)

$$T = \theta_{11}(G\cos\alpha + t\bar{f}_4 \sin\alpha) \equiv \theta_{11}h_{11}(t,G) \tag{54a}$$

$$S = \theta_{11}(G\sin\alpha - t\bar{f}_4 \cos\alpha) \equiv \theta_{11}h_{22}(t,G) \tag{54b}$$

The final form of the entrainment equation is

$$h_{11}\frac{\partial \theta_{11}}{\partial \ell_\phi} + \theta_{11}\frac{\partial h_{11}}{\partial t}\frac{\partial t}{\partial \ell_\phi} + \theta_{11}\frac{\partial h_{11}}{\partial H}\frac{\partial H}{\partial \ell_\phi} + h_{22}\frac{\partial \theta_{11}}{\partial \ell_\theta}$$

$$+ \theta_{11}\frac{\partial h_{22}}{\partial t}\frac{\partial t}{\partial \ell_\theta} + \theta_{11}\frac{\partial h_{22}}{\partial H}\frac{\partial H}{\partial \ell_\theta} = C_3(\theta_{11},t,H) \tag{55}$$

where

$$C_3 = F(H) - \frac{T}{U_s}\frac{\partial U_s}{\partial \ell_\phi} - \frac{S}{U_s}\frac{\partial U_s}{\partial \ell_\theta} + TK_\phi + SK_\theta \tag{56}$$

REFERENCES

1. von Kerczek, C., "Calculation of the Turbulent Boundary Layer on a Ship Hull," Journal of Ship Research, Vol. 17, pp. 106-120 (1973).

2. Landweber, L. and V.C. Patel, "Ship Boundary Layers," to be published in Annual Reviews of Fluid Mechanics, Vol. 12 (1979).

3. Cebeci, T. et al., "A General Method for Calculating Three-Dimensional Laminar and Turbulent Boundary Layers on Ship Hulls," presented at the 12th ONR Symposium on Naval Hydrodynamics, Washington, D.C. (1978).

4. Spalding, D.B., "Theories of the Turbulent Boundary Layer," Applied Mechanics Reviews, Vol. 20 (1967).

5. Green, J.E. et al., "Prediction of Turbulent Boundary Layers and Wakes in Compressible Flow by a Lag-Entrainment Method," Aeronautical Research Council of Great Britain, R and M 3791 (1977).

6. Miloh, T. and V.C. Patel, "Orthogonal Coordinate Systems for Three-Dimensional Boundary Layers with Particular Reference to Ship Forms," Journal of Ship Research, Vol. 17, No. 1 (1973).

7. Myring, D.F., "An Integral Prediction Method for Three-Dimensional Turbulent Boundary Layers in Incompressible Flow," Royal Aircraft Establishment, Technical Report 70147 (1970).

8. Reynolds, W.C. and T. Cebeci, "Calculation of Turbulent Flow," in Topics in Applied Physics, Vol. 12, P. Bradshaw, editor, Springer-Verlag (1976).

9. Cumpsty, N.A. and M.R. Head, "The Calculation of Three-Dimensional Turbulent Boundary Layers, Part 1: Flow Over the Rear of an Infinite Swept Wing," The Aeronautical Quarterly, Vol. 18, pp. 55-84 (1965).

10. Head, M.R. and V.C. Patel, "Improved Entrainment Method for Calculating Turbulent Boundary Layer Development," Aeronautical Research Council (Great Britain), R and M 3643 (1968).

11. Coles, D.E., "The Young Person's Guide to the Data," Proceedings Computation of Turbulent Boundary Layers - 1968, Air Force Office of Scientific Research IFP-Stanford Conference, Vol. II, D.E. Coles and E.A. Hirst, editors (1968).

12. Thompson, J.G., "A New Two-Parameter Family of Mean Velocity Profiles for Incompressible Turbulent Boundary Layers on Smooth Walls," Aeronautical Research Council (Great Britain), R and M 3463 (1976).

13. Mager, A., "Generalization of Boundary-Layer Momentum-Integral Equations to Three-Dimensional Flows, Including Those of Rotating Systems," National Advisory Committee for Aeronuatics Report 1067 (1952).

14. Okuno, T., "Distribution of Wall Shear Stress and Cross Flow in Three-Dimensional Turbulent Layer on Ship Hull," Journal Society Naval Architects of Japan, Vol. 139, pp. 10-22 (1976).

15. von Kerczek, C. and E.O. Tuck, "The Representation of Ship Hulls by Conformal Mapping Functions," Journal of Ship Research, Vol. 13, pp. 284-298 (1969).

16. Chang, M.S. and P.C. Pien, "Hydrodynamic Forces on a Body Moving Beneath a Free Surface," Proceedings of the First International Conference on Numerical Ship Hydrodynamics, J. Schot and N. Salvesen, editors, Gaithersburg (1975).

17. Hess, J.L. and A.M.O. Smith, "Calculation of Nonlifting Potential Flow About Abritrary Three-Dimensional Bodies," Journal of Ship Research, Vol. 8, No. 2 (1964).

18. Alberg, J.H. et al., "The Theory of Splines and Their Applications," Academic Press, New York (1967).

19. O'Brien, G.G. et al., "A Study of the Numerical Solution of Partial Differential Equations," Journal of Mathematics and Physics, Vol. 29, pp. 223-251 (1951).

20. Joubert, P.N. and N. Matheson, "Wind Tunnel Tests of Two Lucy Ashton Reflex Geosims," Journal of Ship Research, Vol. 14 (1970).

21. Larsson, L., "Boundary Layers on Ships, Part IV: Calculations of the Turbulent Boundary Layer on a Ship Model," The Swedish State Shipbuilding Experimental Tank, Göteborg, Sweden, Report 47 (1974).

INITIAL DISTRIBUTION

Copies		Copies	
1	DOD, ARPA, G. Donahue	1	NSWC, Dahlgren/Lib
L	WES	1	NUSC/Lib
1	U.S. ARMY TRAS R&D Marine Trans Div	7	NAVSEA 1 SEA 0322 1 SEA 033 1 SEA 03512/Peirce 1 SEA 037 3 SEA 09G32
1	CHONR/438 Cooper		
2	NRL 1 Code 2027 1 Code 2629	1	NAVFAC/Code 032C
1	ONR/Boston	1	NAVSHIPYD PTSMH/Lib
1	ONR/Chicago	1	NAVSHIPYD PH[illegible]A/Lib
1	ONR/New York	1	NAVSHIPYD NORVA/Lib
1	ONR/Pasadena	1	NAVSHIPYD CHASN/Lib
1	ONR/San Francisco	1	NAVSHIPYD LBEACH/Lib
1	NORDA	2	NAVSHIPYD MARE 1 Library 1 Code 250
3	USNA 1 Tech Lib 1 Nav Sys Eng Dept 1 B. Johnson	1	NAVSHIPYD PUGET/Lib
		1	NAVSHIPYD PEARL/Code 202.32
3	NAVPGSCOL 1 Library 1 T. Sarpkaya 1 J. Miller	8	NAVSEC 1 SEC 6034B 1 SEC 6110 1 SEC 6114H 1 SEC 6120 1 SEC 6136 1 SEC 6140B 1 SEC 6144 1 SEC 6148
1	NADC		
4	NOSC 1 Library 1 T. Lang 1 J.W. Hoyt 1 D.M. Nelson	1	NAVSEC, NORVA/6660.03, Blount
1	NCSC/712, D. Humphreys	12	DDC
1	NCEL/Code 131	1	AFOSR/NAM
1	NSWC, White Oak/Lib	1	AFFOL/FYS, J. Olsen

Copies

2 MARAD
- 1 Div of Ship R&D
- 1 Lib

1 NASA HQS/Lib

3 NBS
- 1 Lib
- 1 P.S. Klebanoff
- 1 G. Kulin

1 NSF/Eng Lib

1 LC/Sci & Tech

1 DOT/Lib TAD-491.1

2 MMA
- 1 National Maritime Research Center
- 1 Library

1 U. of Bridgeport/E. Uram

4 U. of Cal/Dept Naval Arch, Berkeley
- 1 Library
- 1 W. Webster
- 1 J. Paulling
- 1 J. Wehausen

2 U. of Cal, San Diego
- 1 A.T. Ellis
- 1 Scripps Inst Lib

5 CIT
- 1 Aero Lib
- 1 T.Y. Wu
- 1 A.J. Acosta
- 1 I. Sabersky
- 1 D. Coles

1 City College, Wave Hill/ Pierson

1 Catholic U. of Amer./Civil & Mech Eng

1 Colorado State U./Eng Res Cen

Copies

1 U. of Connecticut/Scottron

1 Cornell U./Shen

2 Florida Atlantic U.
- 1 Tech Lib
- 1 S. Dunne

2 Harvard U.
- 1 G. Carrier
- 1 Gordon McKay Lib

1 U. of Hawaii/Bretschneider

1 U. of Illinois/J. Robertson

4 U. of Iowa
- 1 Library
- 1 L. Landweber
- 1 J. Kennedy
- 1 V.C. Patel

1 Johns Hopkins U./Phillips

1 Kansas State U./Nesmith

1 U. of Kansas/Civil Eng Lib

1 Lehigh U./Fritz Eng Lab Lib

5 MIT
- 1 Library
- 1 P. Leehey
- 1 P. Mandel
- 1 M. Abkowitz
- 1 J.N. Newman

4 U. of Minn/St. Anthony Falls
- 1 Silberman
- 1 Lib
- 1 Song
- 1 R. Arndt

4 U. of Mich/NAME
- 1 Library
- 1 F. Ogilivie
- 1 Hammitt
- 1 Cough

Copies	
2	U. of Notre Dame 1 Eng Lib 1 Strandhagen
2	New York U./Courant Inst 1 A. Peters 1 J. Stoker
4	Penn State 1 B.R. Parkin 1 R.E. Henderson 1 J.L. Lumley 1 ARL Lib
1	Princeton U./Mellor
2	U. of Rhode Island 1 F.M. White 1 T. Kowalski
5	SIT 1 Library 1 Breslin 1 Savitsky 1 P.W. Brown 1 Tsakonas
1	U. of Texas/Arl Lib
1	Utah State U./Jeppson
2	Southwest Res Inst 1 Applied Mech Rev 1 Abramson
3	Stanford U. 1 Eng Lib 1 R. Street, Dept Civil Eng 1 S.J. Kline, Dept Mech Eng
1	Stanford Res Inst/Lib
1	U. of Washington/Arl Tech Lib

Copies	
3	VPI 1 H.L. Moses, Dept Mech Eng 1 D.P. Telionis, Dept Mech Eng 1 J. Schetz, Dept Aero & Ocean Eng
3	Webb Inst 1 Library 1 Lewis 1 Ward
1	Woods Hole/Ocean Eng
1	Worchester PI/Tech Lib
1	SNAME/Tech Lib
1	Bethlehem Steel/Sparrows Point
1	Bethlehem Steel/New York/Lib
1	Bolt, Beranek & Newman/Lib
1	Exxon, NY/Design Div, Tank Dept
1	Exxon Math & System, Inc.
1	General Dynamics, EB/ Boatwright
1	Gibbs & Cox/Tech Info
4	Hydronautics 1 Library 1 E. Miller 1 V. Johnson 1 C.C. Hsu
1	Lockheed, Sunnyvale/Waid
2	McDonnell Douglas, Long Beach 1 T. Cebeci 1 J. Hess
1	Newport News Shipbuilding/Lib
1	Nielsen Eng & Res

Copies	
1	Oceanics
3	Rand Corp 1 E.R. Van Driest 1 C. Gazley 1 J. Aroesty
1	Rockwell International/B. Ujihara
1	Sperry Rand/Tech Lib
1	Sun Shipbuilding/Chief Naval Arch
1	Robert Taggart
1	Tracor
2	Westinghouse Electric 1 M.S. Macovsky 1 Gulino

CENTER DISTRIBUTION

Copies	Code	Name
1	11	W.M. Ellsworth
1	117	R.M. Stevens
1	1500	
1	1504	V.J. Monacella
1	1506	M.K. Ochi
1	1507	D. Moran
1	1508	F. Peterson
1	1521	P. Pien
1	1524	Y.T. Shen
1	1524	W.C. Lin
1	1524	W. Day
1	1532	G. Dobay
1	1532	M. Wilson
1	1540	W.B. Morgan
1	1541	P. Granville
1	1542	B. Yim
1	1544	R. Cumming
1	1544	R. Boswell
1	1544	E. Caster
1	1544	S. Jessup
1	1552	T.T. Huang
1	1552	N. Salvesen
30	1552	C. von Kerczek
1	1552	H.T. Wang
1	1552	J. McCarthy
1	1552	T. Langan
1	1560	G. Hagen
1	1562	M. Martin
1	1564	J. Feldman
1	1568	G. Cox
1	1572	M.D. Ochi
1	1572	E. Zarnick
1	1572	C.M. Lee
1	1576	W.E. Smith
1	1615	R.J. Furey
1	184	H. Lugt
1	1843	J. Schot
1	1843	C. Dawson
1	19	M.M. Sevik
1	1942	J.T. Shen
1	1942	W.R. Brown
1	1942	F.C. DeMetz
1	1942	T.M. Farabee
1	1942	F.E. Geib
1	1942	T.C. Mathews
10	5211.1	Reports Distribution
1	522.1	Unclassified Lib (C)
1	522.2	Unclassified Lib (A)